Navigating contradictions: *Salmonella* Typhimurium chemotactic responses to conflicting effector stimuli

Kailie Franco,[a] Zealon Gentry-Lear,[b*] Michael Shavlik,[c] Michael J. Harms,[b,c] Arden Baylink[a#]

[a] Department of Veterinary Microbiology and Pathology, Washington State University, Pullman, Washington, USA

[b] Institute of Molecular Biology, University of Oregon, Eugene, Oregon, USA

[c] Department of Chemistry & Biochemistry, University of Oregon, Eugene, Oregon, USA

[#] Address correspondence to Arden Baylink, PhD, arden.baylink@wsu.edu

[*] Present address: Zealon Gentry-Lear, Department of Microbiology, University of Washington, Washington, USA

Abstract

Chemotaxis controls motility and colonization in many enteric pathogens, yet most studies have examined bacterial responses to single effectors in isolation. Previously, we reported that *Salmonella* Typhimurium uses the chemoreceptor Tsr to detect L-serine (L-Ser) in human blood serum, promoting invasion of damaged vasculature (*Glenn et al., eLife* 2024 [1]). Tsr also mediates sensing of indole, a microbiota-derived chemorepellent and bactericide proposed to protect against enteric infection by deterring pathogen colonization. The major biological reservoir of indole in the gut is feces, where it accumulates to millimolar levels. Here, we tested whether indole-rich human fecal material is protective against infection and found that exposure to feces instead enhances intestinal invasion in an explant model. Surprisingly, diverse non-typhoidal *Salmonella* serovars were strongly attracted to feces despite its high indole content. We found that while pure indole is a strong repellent sensed through Tsr, its effects are overridden in the presence of nutrient attractants, including L-Ser. Moreover, indole only minimally impairs growth in the presence of sufficient nutrients. Using video microscopy, we observed that Tsr integrates L-Ser and indole signals in real time, biasing bacterial movement based on the relative concentrations of attractant and repellent. We propose that this chemotactic compromise optimizes pathogen fitness by guiding bacteria to niches with a favorable L-Ser-to-indole ratio, balancing nutrient acquisition and avoidance of high microbial competitor density. These findings highlight the limitations of single-effector studies in predicting bacterial navigation in complex environments, where chemotaxis is shaped by the integration of multiple, often opposing, chemical cues.

Introduction

Many bacteria that colonize the gastrointestinal tracts of humans and other animals employ chemotaxis to sense chemical effectors in the gut lumen and swim to environments conducive for growth and colonization [2–6]. This process is controlled by chemoreceptor proteins, which recognize chemical effectors and transduce signals through a phosphorylation cascade to regulate flagellar rotation and swimming direction, ultimately determining the spatial and temporal patterns of bacterial colonization (Fig. 1A) [2,3,7,8]. In turn, the colonization topography of bacteria within the gut influences the health of the host through nutrient absorption, developmental regulation, and resistance to pathogens [9–11]. While many effectors have been studied and characterized in isolation as attractants or repellents [5,8], natural environments contain mixtures of opposing signals. In the enteric lumen, bacteria encounter a complex milieu of conflicting effector stimuli, including nutrients, molecular cues, and toxins [2,5]. Only a handful of studies have investigated how bacteria navigate conflicting chemical gradients and there remains much to learn about how bacteria prioritize these signals to direct their movement and colonization (Fig. 1B) [2,5,12–19].

A chemical effector of major importance for enteric bacterial communities is indole, an interbacterial signaling molecule that regulates diverse aspects of physiology and lifestyle [20–22]. Indole is excreted by gut microbiota as a byproduct of tryptophan metabolism and accumulates to millimolar levels in human feces (Fig. 1A-B) [20,23,24]. Indole is amphipathic and can transit bacterial membranes to regulate biofilm formation and motility, suppress virulence programs, and exerts bacteriostatic and bactericidal effects at high concentrations [20–22,24–26]. Indole was one of the earliest identified chemorepellents, and subsequent work has extensively explored its role in *Escherichia coli* chemotaxis (Table S1) [12,13,15,18,22,27]. Recent studies have advanced our understanding of the molecular mechanisms underlying *E. coli* indole taxis and the involvement of the chemoreceptor taxis to serine and repellents (Tsr) (Fig. 1A-B) [12,13,18,22]. From this body of research, the hypothesis emerged that indole from the gut microbiota repels pathogens and restricts their growth as a mechanism of colonization resistance conferred by the microbiome [12,20–22,28,29]. If true, this could represent an interesting avenue for cultivating healthy microbiomes more robust against pathogen infiltration. However, indole taxis has only been studied in *E. coli* and no prior work has tested whether human fecal material, the major biological source of indole in the gut, induces frank pathogen chemorepulsion or inhibits pathogen growth at physiologically relevant levels (Table S1).

69 We were interested in further studying the role of Tsr in navigating contradictory effector
70 stimuli because this chemoreceptor possesses an interesting dual function: it senses
71 chemorepellents and also the amino acid and nutrient L-Ser as a chemoattractant (Fig. 1A-B)
72 [1,2,12,13,18,22,27,30–32]. Tsr plays important roles during enteric invasion [33–35], but questions remain
73 about how the chemoreceptor regulates pathogen colonization in the presence of conflicting
74 signals. We recently mapped the biological distribution of Tsr and reported that many enteric
75 pathogens and pathobionts possess Tsr orthologues, including the genera *Salmonella*, *Citrobacter*,
76 and *Enterobacter* [1]. Whether these and other bacteria respond to indole as a chemorepellent has
77 remained unclear because all prior studies of indole taxis focused on *E. coli* (Table S1). Prior *in*
78 *vitro* work with purified effectors showed when both attractants and repellents are present, Tsr
79 facilitates so-called "intermediate" responses between chemoattraction and chemorepulsion,
80 suggesting that, in some cases, navigating conflicting stimuli is regulated at the single
81 chemoreceptor level [13]. These types of chemotactic compromises, such as those that have been
82 referred to as bet-hedging, trade-off, and simultaneous sensing, remain insufficiently studied, but
83 could be relevant to enteric infections because the gut lumen contains conflicting effectors [13,18,19].
84 Earlier work posited that bacteria sum conflicting signals and ultimately perform attraction or
85 repulsion responses based on the relative concentrations and sensitivity to the individual effectors,
86 which, if true, would enable straight-forward predictions for behaviors to effector mixtures [15,18].
87 But, this binary model of chemotaxis seems too coarse to explain recent observations of population
88 structures that emerge in response to conflicting signals that are clearly distinct from either
89 attraction or repulsion [13,19].
90 In this study, we aimed to gain a deeper understanding into how chemotaxis directs
91 bacterial localization to naturally-occurring stimuli that contain conflicting effectors, the types of
92 population structures that arise and their dynamics of formation, and their potential relevance in
93 enteric infections. *Salmonella enterica* serovar Typhimurium is a frank pathogen that relies on
94 chemotaxis for enteric infection and employs an array of strategies to compete with the native
95 microbiota for nutrients and colonization niches, ultimately invading the intestinal tissue and
96 becoming intracellular [9,33–38]. *S.* Typhimurium also differs fundamentally from *E. coli* because it
97 lacks tryptophanase genes and cannot itself produce indole, and thereby could provide a novel
98 perspective on indole taxis [39,40]. In this study, we used the pathogen *S.* Typhimurium as a model
99 system to: (1) test the hypothesis that the microbiota secretion product indole is protective against

100 enteric invasion, (2) investigate if pathogens are repelled by indole-containing fecal material, and
101 (3) learn how the chemoreceptor Tsr regulates pathogen spatial localization in response to
102 conflicting chemotactic stimuli of the intestinal environ. Using live imaging, we directly visualized
103 how enteric pathogen populations dynamically restructure in response to physiological mixtures
104 of attractants and repellents. We demonstrate that chemotaxis responses to natural biological
105 combinations of effectors, and their impacts on infection outcomes, are not easily predicted based
106 on responses to individual effectors alone.
107
108 **Results**
109 *Impact of opposing chemoeffector stimuli on pathogen invasion in swine colonic explants*
110 We sought to test whether indole in human fecal matter protects against *S.* Typhimurium infection
111 and whether this involves chemorepulsion mediated by the chemoreceptor Tsr. *S.* Typhimurium
112 preferentially invades tissue of the distal ileum, but also infects the cecum and colon [41–44]. We
113 presume the amount of indole is greatest in the lower gastrointestinal tract where tryptophan has
114 been maximally digested by microbiota tryptophanases, and so we developed a swine colonic
115 explant model that mimics the architecture and size of adult human colonic tissue [40,45–49]. We based
116 this model on a prior study of explant tissue used to characterize invasion through gentamicin
117 washes that kill extracellular and attached bacteria [50]; gentamicin washing is also a commonly-
118 used method to quantify *S.* Typhimurium intracellular populations in cell culture experiments [51,52].
119 A section of colonic tissue was prepared for each experiment with gentle cleaning and treated with
120 various effector solutions: solubilized human feces, purified indole and/or L-Ser at fecal-relevant
121 concentrations, or buffer as a control (see Materials & Methods for tissue dimensions and other
122 experiment details). This experimental setup simulates a biological gradient in which the effector
123 concentration is initially highest near the tissue and diffuses outward into the buffer solution.
124 Following treatment with effectors, the tissue was subsequently exposed to co-infection
125 with wild-type (WT) *S.* Typhimurium strain IR715 and either a *cheY* mutant (motile but non-
126 responsive to chemoeffector stimuli) or *tsr* deletion mutant (Fig. 1C-D, Table 1) [33]. The
127 functionality of these mutants have been confirmed through *in vivo* infection studies using
128 genetically complemented strains [33,34]. To assess the role of chemotaxis in infection, we quantified
129 total bacteria harvested from tissue homogenates and also enumerated bacteria following a

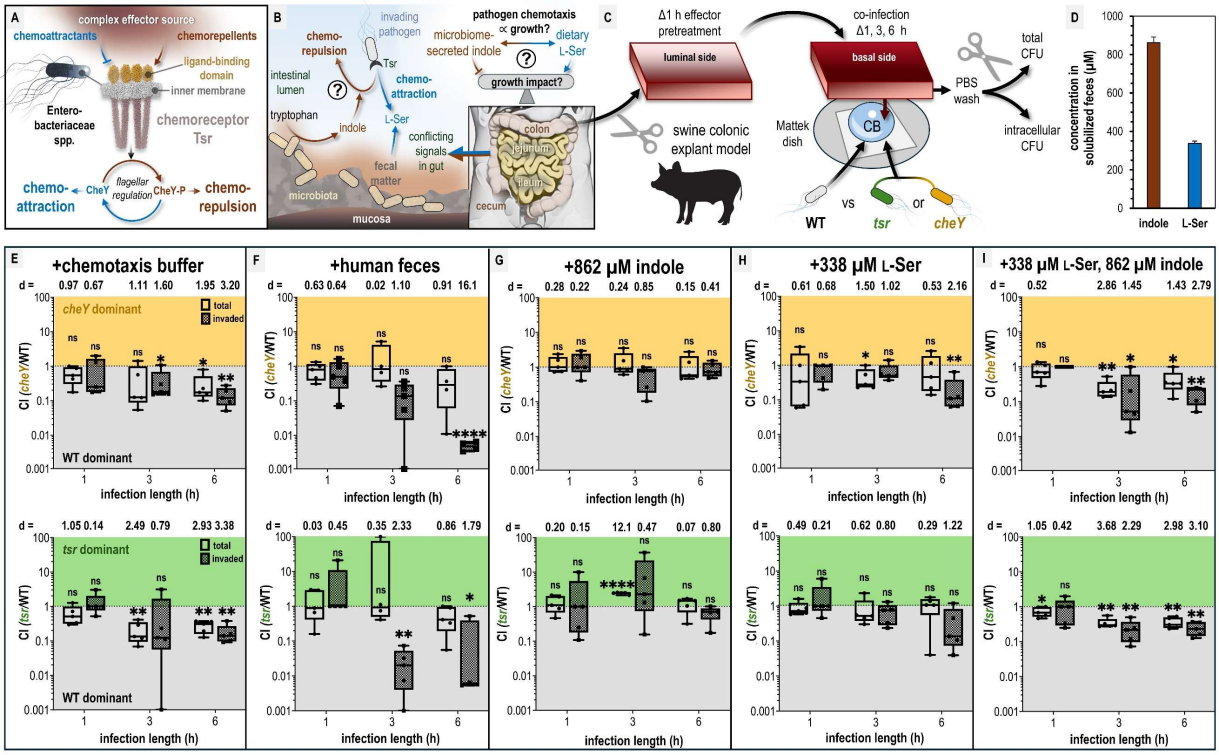

Fig. 1. Tsr and chemotaxis mediate efficient pathogen invasion of colonic tissue. A-B. Overview of the role of Tsr in chemotactic responses and premise of this study. C. Experimental design of colonic explant infections. See Materials & Methods for experiment details such as tissue dimensions. D. Serine (presumed to be nearly 100% L-Ser, see Materials & Methods) and indole content of liquid human fecal treatments, as measured by mass spectrometry. E-I. Competitive indices (CI) of colony-forming units (CFUs) recovered from co-infected swine explant tissue, either from the total homogenate (open box and whiskers plots), or from tissue washed with gentamicin to kill extracellular and attached cells, which we refer to as the "invaded" intracellular population (checkered box and whisker plots), as indicated. Each data point represents a single experiment of a section of tissue infected with bacteria, and the CI of CFUs recovered from that tissue (n=5). Boxes show median values (line) and upper and lower quartiles, and whiskers show max and min values. Effect size (Cohen's *d*) and statistical significance are noted for each experiment in relation to competitive advantage, i.e. deviation from a CI of 1 (not significant, ns; * $p < 0.05$, ** $p < 0.01$, *** $p < 0.001$, **** $p < 0.0001$). See also Figure S1 for disaggregated CFU enumerations for each experimental group prior to CI calculation. Data S1 contains all numerical CFU measurements.

gentamicin wash, which we presume to reflect bacteria that were intracellular and evaded killing by the gentamicin wash, at 1, 3, and 6 h post-infection (Fig. 1C, Materials & Methods) [53,54]. For buffer-treated explant experiments, WT *S.* Typhimurium showed a modest time-dependent advantage in colonization and invasion compared to chemotactic mutants, indicating that chemotaxis, and specifically Tsr, promotes tissue colonization under baseline conditions (Fig. 1E, Fig. S1A-B, Data S1).

136 The hypothesis that indole protects against pathogen colonization predicts that feces, the
137 major biological repository of gut indole, will protect against invasion. Contrary to this, we found
138 that fecal treatment significantly enhances intracellular invasion of WT *S.* Typhimurium
139 (compared to buffer treatment), providing a >100-fold competitive advantage mediated by Tsr
140 (Fig. 1F, Fig. S1C-D). Analysis of the liquified human fecal matter used in this study revealed an
141 indole concentration of 862 μM, consistent with previously reported ranges (0.5–5 mM) (Fig. 1D,
142 Materials & Methods) [20,23–26]. However, when colonic tissue was treated with purified indole at
143 the same concentration, the competitive advantage of WT over the chemotactic mutants was
144 abolished compared to fecal-treated tissue (Fig. 1G, Fig. S1E-F, Data S1). Given that Tsr mediates
145 attraction to L-Ser for both *E. coli* and *S.* Typhimurium, we hypothesized that L-Ser present in
146 feces might be responsible for increased colonization of fecal-treated tissue [1,2,55,56]. However,
147 treatment with 338 μM L-Ser, the concentration present in our fecal sample (Fig. 1D, Materials &
148 Methods), actually shows a decrease in WT advantage compared to fecal treatment, similar to the
149 effect of indole alone (Fig. 1H, Data S1). While treatments with either indole or L-Ser decrease
150 the WT advantage, total bacterial loads are similar, suggesting that neither effector is "protective"
151 in terms of infection burden (Fig. S1, Data S1). Since both effectors individually alter invasion,
152 but do not on their own recapitulate the efficient invasion phenotype observed with fecal treatment,
153 we then wondered whether the combination of indole and L-Ser might be sufficient. Interestingly,
154 we found that treatment with a mixture of indole and L-Ser effectively neutralized their individual
155 effects, resulting in a response nearly identical to buffer-treated tissue, and the WT advantage
156 observed with fecal treatment was not recapitulated (Fig. 1I, Fig. S1I-J, Data S1).
157 These results provide insights into the relationship between chemotactic sensing of fecal
158 material and its role in invasion, while also revealing complex behaviors that raise further
159 questions. The key takeaway is that although pure indole reduces WT colonization advantage in a
160 chemotaxis- and Tsr-dependent manner, indole within feces does not elicit the same response, nor
161 does indole-rich fecal material provide protection against invasion in this model (Fig. 1, Fig. S1).
162 This may be explained by our observation that L-Ser can cancel out the effects of indole (Fig. 1G,
163 Fig. 1I, Data S1). These findings suggest that the presence of multiple chemical signals within
164 complex biological effector sources can make it challenging to predict chemotactic behavior based
165 on how the bacteria respond to singular effectors.

166 Curiously, when L-Ser and indole are present together, the magnitude of the WT advantage
167 over the *cheY* and *tsr* mutants resembles a null response (i. e. similar to buffer treatment), rather
168 than providing an additive fitness advantage like occurs with fecal treatment (Fig. 1, Data S1). One
169 possible explanation is that fecal material contains other metabolites that influence sensing and
170 growth [2,8,57–61]. Additionally, the WT advantage in the presence of fecal material could relate to
171 Tsr-mediated energy taxis [33,34], swimming regulation that encourages invasion [38], or experimental
172 treatment conditions that may impact bacterial growth. To further investigate these behaviors, the
173 following sections examine chemotactic responses to these treatments and their effects on growth.
174
175 *Non-typhoidal S. enterica are attracted to human feces despite high indole content*
176 Having found that Tsr mediates efficient colonic invasion for *S.* Typhimurium in our explant
177 system when exposed to fecal material, we next sought to learn what chemotactic behaviors this
178 chemoreceptor orchestrates in response to feces; given that this represents the highest
179 concentration of indole *S.* Typhimurium might natively encounter, we expected to observe
180 chemorepulsion (Fig. 1D, Table S1) [12,13,18,27,32]. We employed the chemosensory injection rig assay
181 (CIRA) for live-imaging of bacterial chemotaxis responses to a source of effectors injected through
182 a glass microcapillary [1]. The flow and dynamic nature of the gut lumen make this a suitable
183 approach for modeling and studying enteric chemotaxis responses *in vitro* [1].
184 In this assay, chemoattraction is observed as an influx of cells toward the effector source
185 and chemorepulsion as decreasing cells (Figure S2). As described previously, effector injection
186 introduces a steep microgradient, and, using mathematical modeling of the diffusion of the fecal
187 sources of indole and L-Ser, we can approximate the local concentrations experienced by bacteria
188 at a given distance from the injection source, which for most of the field of view is in the picomolar
189 to low nanomolar range (Fig. 2A, Materials & Methods) [1]. Using experiments with fluorescent dye
190 we previously confirmed our calculated local effector concentrations to be in the range of 5-10%
191 within 300 μm of the injection source [1]. Further, we showed using a set of controls of buffers at
192 different pH, and chemotaxis mutants, that the low flow-rate of our apparatus (approximately 300
193 femtoliters per minute) does not itself meaningfully perturb the bacterial population relative to the
194 much larger shifts that occur due to chemotaxis responses [1].
195 Over five minutes, we found both WT and *tsr* exhibit strong chemoattraction to fecal

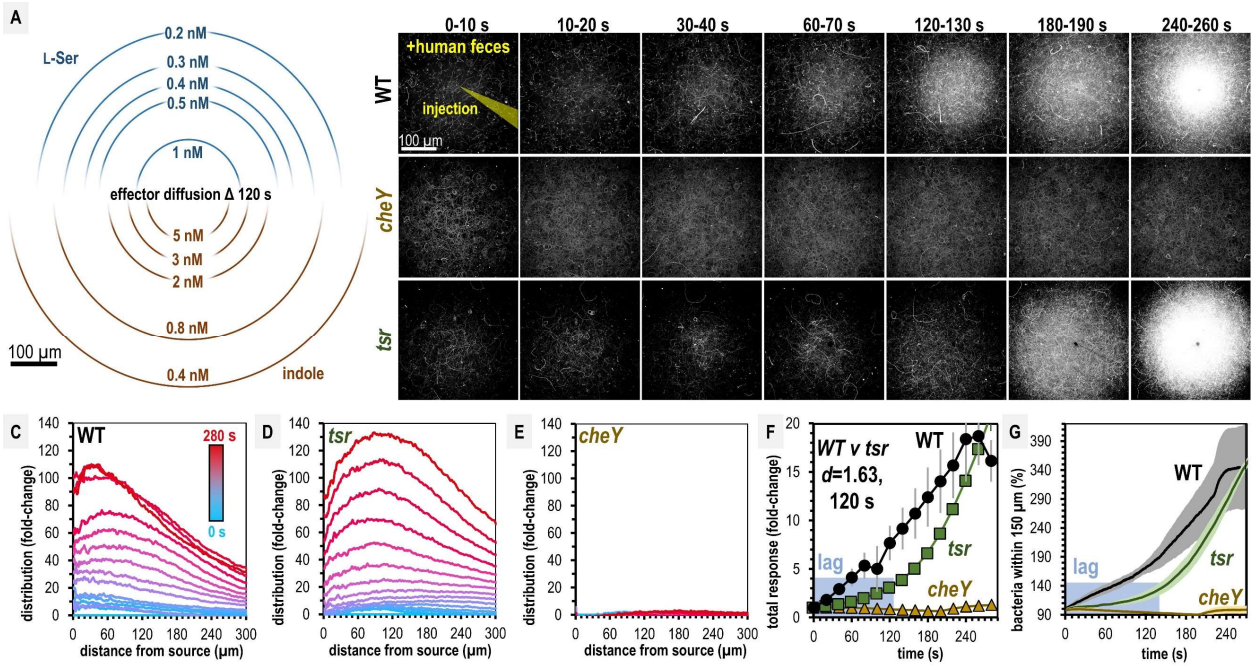

Fig. 2. *Salmonella* Typhimurium exhibits attraction toward liquid human fecal material. A. Diffusion modeling showing calculated local concentrations in CIRA experiments with liquid human fecal material based on distance from the central injection source. B. Max projections of representative *S.* Typhimurium IR715 responses to a central source of injected liquid human fecal material. C-E. Bacterial population density over time in response to fecal treatment. The initial uniform population density in these plots is indicated with the blue line (time 0), and the final mean distributions with the red line (time 280 s), with the mean distributions between these displayed as a blue-to-red spectrum at 10 s intervals. F-G. Temporal analyses of area under the curve (AUC) or relative number of bacteria within 150 µm of the source. Effect size (Cohen's *d*) comparing responses of WT and *tsr* attraction at 120 s post-treatment is indicated. Data are means and error bars are standard error of the mean (SEM, n=3-5). See also Movie 1, Table S1, and Figure S2.

196 material, whereas *cheY* remains randomly distributed (Fig. 2B, Movie 1). By examining the radial
197 distribution of the bacterial populations, we found WT more tightly centers around the treatment
198 source than *tsr* (Fig. 2C-E, Movie 1). In terms of the rate of bacterial accumulation, the
199 chemoattraction of *tsr* lags behind the WT for the first 120 s (Fig. 2F-G, Movie 1). We wondered
200 how these deficiencies in fecal attraction might translate to direct competition, where different
201 strains are experiencing the same treatment source simultaneously. To address this, we performed
202 CIRA with solubilized human feces and two strains present in the same pond, which we tracked
203 independently through fluorescent markers (Fig. 3) [1]. As expected, WT shows a strong
204 chemoattraction response versus *cheY* (Fig. 3A, Movie 2). Interestingly, we found that when
205 competed directly, WT vastly outperforms *tsr*, with the maximal bacterial distribution in proximity

206 to the treatment source higher by about 4-fold (Fig. 3B, Movie 2). These data confirm that despite
207 its high indole content, *S.* Typhimurium is attracted to human fecal material through chemotaxis,
208 and this response involves Tsr, although not as the sole mediator. We expect the attraction of the
209 *tsr* mutant is explained by the fact that *S.* Typhimurium possesses other chemoreceptors that detect
210 glucose, galactose, and L-Asp as chemoattractants, which are present in human feces [2,8,57–61].
211 Recent work highlights how genetic diversity among strains and differences in Tsr
212 expression, even within isogenic populations, modulate chemotaxis function [13,35]. To gain a
213 broader perspective on fecal taxis, we examined the responses among diverse *Salmonella* serovars
214 and strains responsible for human infections. Using dual-channel imaging, we compared *S.*
215 Typhimurium IR715 with a clinical isolate of *S.* Typhimurium, SARA1, and found both strains
216 exhibit attraction to feces, although SARA1 shows a slightly weaker response (Fig. 3C, Movie 3).
217 We then tested a clinical isolate of *S.* Newport, an emerging cause of salmonellosis in the United
218 States and Europe [62,63]. This strain is strongly attracted to fecal material, with a tighter
219 accumulation of cells at the treatment source than *S.* Typhimurium IR715 (Fig. 3D, Movie 3).
220 Lastly, we examined a clinical isolate of *S.* Enteritidis, a zoonotic pathogen commonly transmitted
221 from poultry, which displays weak attraction to fecal material (Fig. 3E, Movie 3) [63]. Overall, we
222 found that chemoattraction to fecal material is conserved among diverse non-typhoidal *Salmonella*
223 serovars responsible for human infections, although the degree of attraction varies. Notably,
224 despite the high indole content in feces, none of the strains tested exhibit chemorepulsion.
225
226 *Mediation of opposing chemotactic responses by Tsr*
227 We wondered if our inability to observe repulsion from fecal material might be due to *S.*
228 Typhimurium not sensing indole as a chemorepellent, since this chemotactic response has only
229 been previously described for *E. coli* (Table S1). We again employed CIRA to address this
230 question, comparing chemotaxis responses to either 5 mM L-Ser or 5 mM indole, and found that
231 *S.* Typhimurium responds rapidly to these two effectors as chemoattractants and chemorepellents,
232 respectively (Fig. S2H-I). Treatment with 5 mM indole, a concentration at the upper end of what
233 occurs in the human gut [26], induces rapid chemorepulsion with the bacteria vacating the region
234 proximal to the source (Fig. S2B). Interestingly, the chemorepulsion response occurs faster than

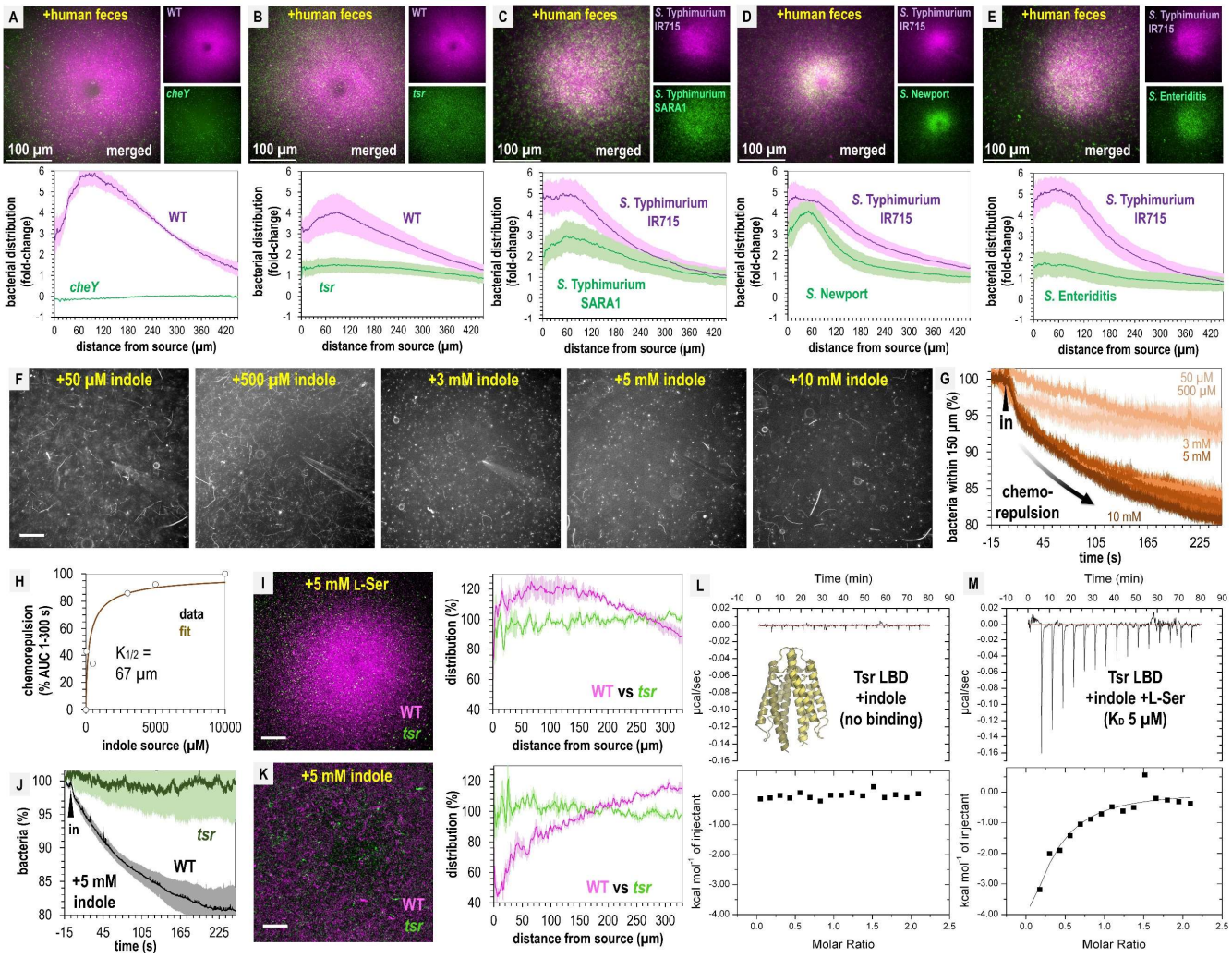

Fig. 3. Fecal indole is insufficient for chemorepulsion but indole in isolation is a strong chemorepellent. A-E. Dual-channel imaging of chemotactic responses to solubilized human feces by WT *S.* Typhimurium IR715 (pink) and isogenic mutants or clinical isolate strains (green), as indicated. Shown are max projections at time 295-300 s post-treatment. Data are means and error bars are standard error of the mean (SEM, n=3-5). See also Movies 2-3. F. Representative max projections of responses at 295-300 s of indole treatment. G-H. Quantification of chemorepulsion as a function of indole concentration (n=3-5). I-K. Comparison of WT and *tsr* mutant responses to L-Ser or indole. See also Fig. S2. L-M. Isothermal titration calorimetry (ITC) experiments with 50 µM *S.* Typhimurium Tsr ligand-binding domain (LBD) and indole, or with L-Ser in the presence of 500 µM indole. Data are means and error bars are standard error of the mean (SEM, n=3-5). AUC indicates area under the curve. Scale bars are 100 µm. See also Movies 2-3.

235 chemoattraction, with a zone of avoidance clearly visible within the first 10 s of indole exposure
236 (Fig. S2I, Movie 4).

237 We next wondered if perhaps our fecal treatments contained insufficient indole to elicit
238 chemorepulsion from *S.* Typhimurium. To identify the effective source concentrations that drive
239 indole chemorepulsion and understand the temporal dynamics of this response, we performed a

240 titration of indole across 0.05-10 mM (Fig. 3F). At all concentrations tested, indole induces
241 chemorepulsion, and the bacteria avoid the treatment source for the duration of the 5-minute
242 experiment (Fig. 3F-G). At source concentrations exceeding 3 mM, essentially all motile cells
243 vacate the field of view within 60 s (Fig. 3F-G). Integrating these chemorepulsion responses and
244 fitting them to a Monad curve suggests an indole source concentration of approximately 67 μM is
245 sufficient for half-maximal ($K_{1/2}$) chemorepulsion (Fig. 3H). These data show that even though we
246 observe strong attraction to fecal material, pure indole at the concentration present in fecal
247 material, and far lower, is indeed a strong chemorepellent for *S.* Typhimurium.

248 Based on its function in *E. coli*, we hypothesized that both indole chemorepulsion and L-
249 Ser chemoattraction for *S.* Typhimurium could be partly or fully mediated through Tsr [8,12,31]. We
250 compared the chemotactic responses of the WT and *tsr* strains when exposed to sources of these
251 effectors and found Tsr to be required for both chemorepulsion from indole and chemoattraction
252 to L-Ser (Fig. 3I-K). The canonical mode of chemoreceptor effector recognition involves binding
253 of the effector to the ligand-binding domain (LBD) [8,64], but the mechanism by which indole is
254 sensed through Tsr in *Salmonella* has not been elucidated. We recently reported the first crystal
255 structure of *S.* Typhimurium Tsr LBD, which clearly defines how the binding site recognizes the
256 L-Ser ligand (PDB code: 8fyv), and we thought it unlikely indole can be accommodated at the
257 same site [1]. To our knowledge, no prior study has tested whether the Tsr LBD binds indole directly,
258 so we expressed and purified the LBD, corresponding to the soluble periplasmic portion, and
259 performed isothermal titration calorimetry (ITC). These data show that no binding occurs between
260 the Tsr LBD and indole (Fig. 3L).

261 We next wondered if indole acts as an allosteric regulator of the LBD, possibly through
262 interacting with the L-Ser-bound form or interfering with L-Ser recognition. To address these
263 possibilities, we performed ITC of 50 μM Tsr LBD with L-Ser in the presence of 500 μM indole
264 and observed a robust exothermic binding curve and K_D of 5 μM, identical to the binding of L-Ser
265 alone (Fig. 3M) [1]. These data indicate that indole does not alter the Tsr LBD affinity for L-Ser. We
266 conclude that Tsr senses indole through an atypical mechanism, which might either involve
267 regulation through a solute-binding protein [12,65], responsiveness to perturbation in the proton motor
268 force [22], or binding to a different region other than the periplasmic LBD. Our findings reveal that
269 while indole acts as a chemorepellent for *S.* Typhimurium in isolation, sensed through Tsr, its
270 presence within fecal material mixed with other effectors is insufficient to elicit chemorepulsion.

Compromising between conflicting effector signals through chemohalation

Earlier work with *E. coli* revealed that exposure to mixtures of L-Ser and indole can elicit intermediate chemotactic responses between chemoattraction and chemorepulsion after prolonged exposure (1-6 h, Table S1) [13]. Having confirmed that Tsr in *S.* Typhimurium mediates opposing responses to the chemoattractant L-Ser and the chemorepellent indole in isolation, we next sought to learn how the bacterial population behaves on rapid timescales when confronted with physiological combinations of these effectors. To address this, we performed a series of CIRA experiments with 500 μM L-Ser and increasing concentrations of indole at L-Ser:indole molar ratios of 10:1, 1:1, or 1:10 (Fig. 4A-D, Movie 4).

These experiments reveal a fascinating transition in the distribution of the pathogen population as a function of increasing chemorepellent, which occurs within minutes of exposure

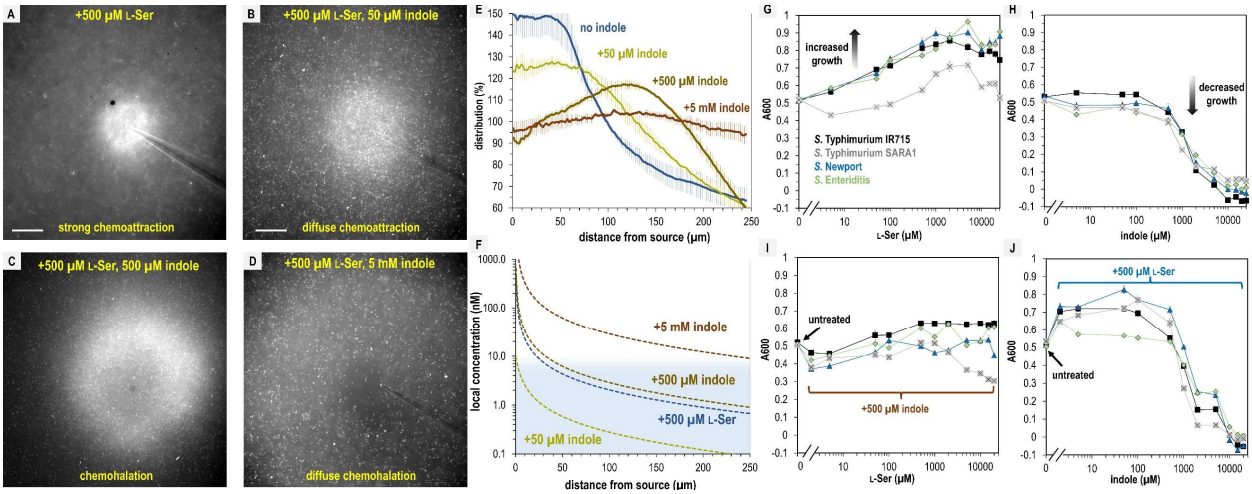

Fig. 4. *S.* Typhimurium mediates distinct chemotactic responses based on the ratio of L-Ser to indole. A-D. Representative max projections of responses to treatments of L-Ser and indole at 295-300 s, as indicated. Scale bars are 100 μm. E. Relative bacterial distribution in response to treatments of 500 μM L-Ser and varying amounts of indole, from panels A-D, with the mean value normalized to 100%. Data are means and error bars are standard error of the mean (SEM, n=3-5). F. Diffusion modeling of local effector concentrations based on sources of 5 mM indole (dark brown), 500 μM L-Ser (blue), 500 μM indole (light brown), and 50 μM indole (yellow) are shown as dashed lines. The approximate local concentration of indole that elicits a transition in chemotactic behavior is highlighted in light blue. G-H. Bacterial growth as a function of L-Ser or indole, at the time point where the untreated culture reaches A_{600} of 0.5. I-J. Bacterial growth +/- pretreatment with 500 μM indole or L-Ser, and increasing concentrations of indole or L-Ser, as indicated at the time point where the untreated culture reaches A_{600} of 0.5. Data are means and error bars are standard error of the mean (SEM, n=8-24).

283 (Fig. 4A-D, Movie 4). With only chemoattractant present, the bacterial population organizes
284 tightly around the effector source (Fig. 4A, Movie 4). When indole is introduced at a concentration
285 10-fold lower than L-Ser, the bacterial distribution still exhibits chemoattraction but becomes more
286 diffuse (Fig. 4B, Movie 4). At a 1:1 ratio of chemoattractant and chemorepellent, a novel
287 population structure emerges, in which the swimming bacteria are attracted toward the source but
288 form a halo around the treatment with an interior region of avoidance (Fig. 4C, Fig. 4E, Movie 4).
289 When the concentration of indole is 10-fold higher than L-Ser, the bacteria exhibit a wider zone of
290 avoidance (Fig. 4D-E, Movie 4). Interestingly, whereas 5 mM indole on its own induces strong
291 chemorepulsion (Fig. S2I, Movie 4), the addition of 10-fold lower L-Ser effectively converts the
292 behavior to a null response (Fig. 4D-E, Movie 4). This demonstrates that even at the highest
293 concentrations of indole *S.* Typhimurium might encounter in the gut, the presence of
294 chemoattractant can override indole chemorepulsion.

295 The intermediate responses to opposing effector mixtures bear similarities to CIRA
296 experiments with fecal material, some of which also exhibited a halo-like structure around the
297 treatment source (Fig. 2, Fig. 3A-E, Movies 2-3). As mentioned earlier, previous studies have also
298 observed responses that are neither attraction nor repulsion, and they have been referred to by a
299 variety of names. We do not claim here that the responses we observe to mixtures of L-Ser and
300 indole are wholly distinct or unrelated to earlier work [13,18,19], but to our knowledge, no other study
301 has so clearly captured the spectrum of behaviors that occur in the transition between attraction
302 and repulsion (Movie 4). There exists no consensus term for taxis of this nature, and so we suggest
303 "chemohalation," in reference to the halo formed by the cell population, and which is congruent
304 with the commonly-used terms chemoattraction and chemorepulsion. We expect chemohalation is
305 a compromise in positional location at the population level between the chemoattraction driven by
306 L-Ser and the chemorepulsion driven by indole. Across these experiments, the interior zone of
307 avoidance roughly corresponds to where the local concentration of indole exceeds 10 nM (Fig. 4E-
308 F). In a biological setting, we presume that the distribution bias orchestrated by chemohalation
309 regulates the probability that cells will colonize, adhere, and transition to sessility at a given site;
310 the greater the local indole content, the wider the zone of avoidance and the less likely tissue
311 invasion occurs.

312 We questioned why non-typhoidal *Salmonella* are attracted to a biological solution with
313 high amounts of indole, a chemical reported to inhibit bacterial growth [21,66,67]. We examined how

314 bacterial growth is affected by 0-25 mM indole or L-Ser in a background of minimal media (MM,
315 Materials & Methods). As expected, increasing amounts of the nutrient L-Ser provide a growth
316 advantage for all *Salmonella* strains analyzed, with maximal benefit achieved by approximately
317 500 μM (Fig. 4G). Equivalent treatments with indole show tolerance up to approximately 1 mM,
318 with growth inhibition occurring in the 1-5 mM range and lethality occurring at indole
319 concentrations greater than 5 mM (Fig. 4H). However, adding L-Ser in a background of 500 μM
320 indole provides only a small growth enhancement (Fig. 4I), and addition of 500 μM L-Ser increases
321 tolerance for indole up to about 1 mM, above which indole toxicity is unavoidable (Fig. 4J). So,
322 we conclude that mixtures of these effectors also impact growth differently than the effectors in
323 isolation, and the relative attraction to combinations of these effectors relates to their propensity
324 to enhance or inhibit growth. Overall, the bacteria still obtain growth benefits from L-Ser so long
325 as the concentration of indole is under 1 mM, and we expect this growth advantage is even greater
326 in the presence of the many other nutrients accessible to the bacteria in fecal material.
327
328 **Discussion**
329 Bacteria in the human gastrointestinal tract encounter complex chemical landscapes that contain
330 both chemoattractants and chemorepellents. However, chemotaxis responses are often studied in
331 isolation, outside of their biological and ecological contexts, which can lead to an over- or
332 underestimation of the roles specific interactions play in natural settings. In the present work, we
333 contribute to an emerging understanding that bacteria exhibit rapid and well-orchestrated
334 responses to conflicting stimuli distinct from chemoattraction or chemorepulsion, and relate these
335 chemotactic compromises to enteric infection and pathogen growth (Fig. 5) [13,19,68]. In this study,
336 we provide evidence that despite the microbiota metabolite indole being a strong repellent in
337 isolation, fecal indole is insufficient to elicit pathogen repulsion or protect against invasion.
338
339 *New insights into indole taxis from a non-E. coli system*
340 Indole is an important and abundant regulator of enteric microbial communities known to modulate
341 motility and virulence and has been proposed to deter pathogen invasion through chemorepulsion
342 [12,20–22,25,26,28,29]. Previously, no study had addressed whether bacteria other than *E. coli* sense indole
343 as a chemorepellent. In the model system we investigated, we confirm that *S.* Typhimurium utilizes
344 the chemoreceptor Tsr to respond to indole as a chemorepellent (Fig. 3). Further, we add to the

345 understanding of indole taxis by having visualized and measured the rapid temporal dimension of
346 indole repulsion, which is relevant in the highly turbulent intestinal environment where bacteria
347 experience shifting and dynamic chemical gradients [1,2]. We found naïve *S.* Typhimurium are
348 repelled from indole sources within 10 s of exposure. The rapidity of this response, which exceeds
349 that of attraction to L-Ser, has not been previously reported (Fig. 3G). We also tested whether
350 indole-sensing occurs through the canonical chemoreceptor mechanism of direct binding through
351 the Tsr LBD, which does not seem to occur, nor does antagonism or inhibition of binding of L-Ser
352 to the LBD (Fig. 3L-M). These data support that a non-canonical sensing mechanism is employed
353 by Tsr to respond to indole, as suggested by others [12,22,65].
354 Having characterized and confirmed the role of Tsr in indole-sensing for *S.* Typhimurium,
355 and shown it to be generally similar to its function in *E. coli* [12,13,18], we can speculate that the
356 diverse bacterial species that possess Tsr orthologues, particularly common among
357 *Enterobacteriaceae* [1], also sense, and are repelled, by indole, further supporting indole as a key
358 regulator of polymicrobial communities of the gut [21,25]. However, *in vivo* Tsr-mediated indole-
359 sensing is integrated with L-Ser-sensing and responses to other stimuli. As discussed further below,
360 this integration may serve to bias colonization toward specific niches based on the local attractant-
361 to-repellent ratio, rather than triggering the outright repulsion we observe *in vitro* with pure indole
362 sources (Fig, 5). While Tsr appears to function similarly in coordinating indole taxis in both *S.*
363 Typhimurium and *E. coli*, its impact on colonization is likely different. Unlike *Salmonella*, *E. coli*
364 produces indole [39,40], which may allow it to use indole not only to regulate colonization based on
365 microbiota activity but also as a self-sensing signal. This could enable *E. coli* to regulate its
366 dispersal or expansion in response to self-generated indole.
367
368 *Indole taxis amidst opposing stimuli and implications for pathogen invasion*
369 We investigated the chemotaxis behaviors of *S.* Typhimurium to human fecal material as a test
370 case for how pathogens make decisions when faced with biological sources of effectors that
371 contain a mixture of conflicting stimuli (Fig. 1, Fig. 2). We predicted that feces, rich in indole,
372 would elicit chemorepulsion, inhibit pathogen growth, and protect against infection [12,20–22,25,28,29].
373 Instead, we find that chemotactic sensing of human fecal material promotes colonic invasion in an
374 explant model, and liquid feces predominantly elicits chemoattraction or chemohalation (Fig. 1,
375 Fig. S1, Fig. 2, Movies 1-S). We also find that while both invasion and chemotaxis are regulated

376 by the presence of the fecal effectors indole or L-Ser alone, these effectors in combination cancel
377 out, leading to a null response (Fig. 1, Fig. 4). These findings help clarify why indole-rich fecal
378 material does not trigger repulsion or prevent invasion. While indole is abundant in feces, it is only
379 one component within a complex biological mixture, and other effectors ultimately mediate
380 chemoattraction or chemohalation to fecal material (Fig. 5).
381 To better understand how chemotaxis responses change when sensing mixtures of opposing
382 effectors, we examined bacterial behavior *in vitro* in the presence of physiological mixtures of the
383 fecal metabolites indole and L-Ser and captured a series of real-time videos (Fig. 4A-D, Movie 4).
384 These videos reveal how, upon sensing the conflicting stimuli, the pathogen population structure
385 rapidly evolves based on the ratio of attractant to repellent, ranging from chemoattraction, diffuse
386 chemoattraction, chemohalation, diffuse chemohalation, and chemorepulsion (Fig. 4A-D, Fig. 5,
387 Fig. S2, Movie 4). We found particularly interesting the response we refer to as chemohalation,
388 which occurs when the bacteria encounter near equimolar attractant and repellent. Under these
389 conditions, the cells accumulate at a distance from the treatment source and form a halo with an
390 interior zone of avoidance (Fig. 3, Movie 4). The zone of avoidance apparently increases as a
391 function of increasing indole, thereby biasing cells against colonizing and invading a specific niche
392 (Fig. 5A). Whereas we observe chemohalation *in vitro* with only two fecal metabolites, we expect
393 this mechanism is at play when the bacteria are selecting among niches in the intestinal lumen,
394 where the indole repulsion signal is integrated alongside information about nutrient attractant
395 signals to ultimately coordinate contact with, and invasion of, intestinal tissue (Fig. 5A).
396
397 *Potential roles for chemohalation in gastrointestinal infections*
398 The dynamic micron-scale chemohalation population structures, that in effect are a compromise
399 between attraction and repulsion, would be difficult or impossible to detect without directly
400 viewing them through live imaging, which may explain why they were unappreciated earlier in
401 binary models of chemotaxis [15]. To be clear, we suggest chemohalation as a useful term to
402 generally describe intermediate chemotaxis responses to conflicting stimuli that are neither
403 chemoattraction nor chemorepulsion, but others have also contributed to studying how chemotaxis
404 functions in confounding chemical landscapes [13,18,19]. The chemohalation responses we report here
405 are most similar to what was referred to as a "trade-off" response in a prior study with *E. coli* and
406 attractant-repellent mixtures; interestingly those authors also observed another response termed

407 "bet-hedging" where a portion of the population within an isogenic culture remained attracted
408 despite the presence of the chemorepellent, but we did not observe this behavior in our experiments
409 [13]. For *S.* Typhimurium, the source concentration required for half-maximal responses are similar
410 for the opposing effectors, 105 and 67 μM for L-Ser [1] and indole, respectively, but the presence of
411 other attractants in feces overall biases behavior toward attraction [57–59,61].

412 In the context of non-typhoidal *Salmonella* infections, it is clear there exists complex
413 relationships between chemotactic sensing of effectors, bacterial growth, and invasion. As it
414 pertains specifically to sensing the opposing effectors L-Ser and indole, we propose that Tsr
415 functions to measure the ratio of exogenous attractant to repellent, and, through chemohalation,
416 orchestrates an appropriate spatial bias in the population. Ultimately, this serves to improve
417 pathogen fitness through colonizing niches rich in nutrients, signaled by local L-Ser
418 concentrations, while avoiding niches with high microbial competition, indicated by local indole
419 concentrations (Fig. 5). Chemorepulsion from indole can be overridden by the presence of
420 chemoattractants, and *S.* Typhimurium growth is quite tolerant of indole within physiological
421 ranges, suggesting the bacteria generally prioritize nutrient acquisition over the inhibitory effects
422 of indole (Fig. 4). This agrees with the premise that nutrient-seeking, rather than avoidance of
423 toxins, may generally be the major function of chemotaxis [6,18]. We expect that the distinction
424 between chemoattraction and chemohalation, in terms of regulating colonization and infection
425 outcomes, also depends on the duration of stimuli exposure and adaptation [12]. Based on data from
426 colonic explant experiments, chemotaxis studies, and growth analyses, we propose a new model
427 describing how the opposing signals from L-Ser and indole are sensed and integrated by Tsr to
428 mediate pathogen invasion (Fig. 5). In addition to sensing of these two effectors, our data support
429 that Tsr and chemotaxis are involved in L-Ser and indole-independent functions in the presence of
430 fecal material that mediate colonization (Fig. 1). This could potentially relate to other characterized
431 functions of Tsr in redox and energy taxis and/or biasing swimming toward a running phenotype,
432 which is associated with increased invasion [33,34,38].

433 Recently, we reported on *Enterobacteriaceae* chemotactic sensing of blood serum, another
434 complex biological effector source at the host-pathogen interface, and those responses appear to
435 involve chemohalation [1]. Evidence of chemohalation is also seen in the case of the gastric pathogen
436 *Helicobacter pylori* responding to mixtures of urea, a chemoattractant, and acid, a chemorepellent
437 [19,69]. Continuing to investigate chemohalation behaviors and understanding how they coordinate

438 bacterial colonization may provide important insights into how chemotaxis confers fitness
439 advantages in natural environments.
440
441 *Limitations of this study*
442 This study provides insights into the roles of chemotaxis in *Salmonella* responses to fecal material
443 and indole; however, several limitations should be considered. First, our experiments were
444 conducted *in vitro* and utilized swine tissue explants, which do not fully capture the complexities
445 of *in vivo* infection dynamics in the human gut. Additionally, while explant assays provided insight
446 into how chemotaxis relates to tissue colonization, these experiments exhibited variability. To
447 mitigate this, we used multiple sections of tissue from a single animal to exert greater experimental
448 control of the system, but this approach limits our ability to assess how host tissue diversity might
449 influence bacterial responses. It would be interesting to assess invasion using tissue of the distal
450 ileum, a major site of *S.* Typhimurium invasion, which is known to have distinct chemical cues
451 and foreseeably differences in indole and L-Ser [41]. Another experimental limitation is the
452 difference in timescales between our assays. Chemotaxis experiments were conducted over short
453 time frames, whereas tissue explant experiments required longer incubation periods for significant
454 differences in colonization and invasion to be observed. Lastly, while we confirmed that non-
455 typhoidal *Salmonella* are attracted to human fecal material, we only determined the dependency
456 on Tsr in our model strain (IR715). Although we expect that other WT clinical isolates also rely
457 on chemotaxis and Tsr for attraction, this remains uncertain without targeted genetic analyses in
458 each strain background.

459

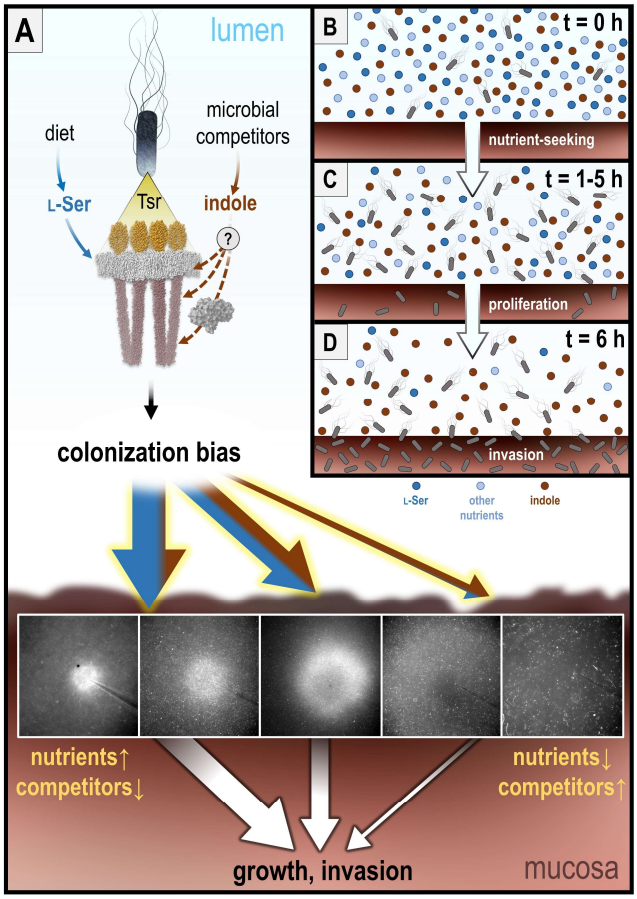

Fig. 5. A. Working model for chemotactic compromise orchestrated by Tsr during enteric invasion. In the intestinal lumen, fecal material contains the nutrient L-Ser, derived from digested food, and bacteriostatic indole, secreted by the gut microbiota. Tsr detects these metabolites as chemoattractant (L-Ser, dark blue arrows) and chemorepellent (indole, brown arrows) signals, respectively. While L-Ser is directly sensed by Tsr via the ligand-binding domain (LBD, yellow), indole is detected through a different mechanism. Tsr integrates these conflicting signals to bias colonization through a behavior termed chemohalation, which promotes taxis toward regions with higher L-Ser-to-indole ratios (large blue and brown arrows, width of arrows denotes the degree of colonization bias). Increased indole levels result in a larger central zone of avoidance and greater bias against colonization. B. During early infection, the attractant-to-repellent ratio in the intestinal lumen is high. *S.* Typhimurium (gray cells) uses chemotaxis to seek L-Ser (dark blue circles) and other nutrients (light blue circles), promoting proliferation. In the presence of abundant nutrients, the bacteria tolerate exposure to indole (brown circles). C. As infection progresses, nutrient consumption by the proliferating bacteria reduces the attractant-to-repellent ratio in the lumen. D. Once nutrients are sufficiently depleted, the bacteria can no longer tolerate indole exposure, and chemorepulsion from indole increases. This repulsion drives bacteria out of the lumen and into contact with the intestinal mucosa, promoting colonic invasion. In the artificial scenario where only L-Ser is present, chemotaxis offers little advantage for invasion; the bacteria proliferate, but there is no incentive to leave the lumen. Conversely, with only indole present, chemotaxis similarly provides no advantage; although indole repels the bacteria from the lumen, it inhibits bacterial proliferation. In the presence of L-Ser, and likely other attractants, indole repulsion is nullified.

460 **Materials & Methods**

461 All methods were carried out in accordance with relevant guidelines, regulations, and state and
462 federal law. Experimental protocols were approved by the Institutional Biosafety Committee (IBC)
463 of Washington State University (#1372).
464
465 *Bacterial strains and growth conditions*
466 Bacterial strains and plasmids used in this study are listed in Table 1. As previously described [1],
467 bacteria intended for chemotaxis assays were grown overnight in tryptone broth (TB) with
468 antibiotic selection, as appropriate. Motile bacteria were prepared with a 1:1000 back-dilution and
469 grown shaking for approximately 4 hours at 37˚ C to reach A_{600} of 0.5. Cells were centrifuged,
470 washed, and resuspended in a chemotaxis buffer (CB) containing 10 mM potassium phosphate
471 (pH 7), 10 mM sodium lactate, and 100 µM EDTA to A_{600} of 0.2 and rocked gently at room
472 temperature until fully motile. For *in vitro* growth analyses, cultures were grown overnight in
473 Lysogeny Broth (LB) at 37˚ C. Subsequently, 5 µl of A_{600} 2.0 cells were used to inoculate 200 µl
474 of minimal media (MM), containing 47 mM Na_2HPO_4, 22 mM KH_2PO_4, 8 mM NaCl, 2 mM
475 $MgSO_4$, 0.4% glucose (w/v) 11.35 mM $(NH_4)_2SO_4$, 100 µM $CaCl_2$ and L-Ser and/or indole at the
476 described concentrations, and cultured in a 96-well microtiter plate. Cultures were grown at 37˚ C
477 and monitored by A_{600} readings at 5-minute intervals.
478

Table 1: Bacterial Strains

Strain	*Reference/Source*
S. enterica Typhimurium IR715 nalidixic acid derivative of ATCC 14028	Rivera-Chávez, F. et al.[33]
S. enterica Typhimurium IR715 Δ*cheY::Tn10* (Tet^R)	Rivera-Chávez, F. et al.[33]
S. enterica Typhimurium IR715 Δ*tsr::pFR3* (Cm^R)	Rivera-Chávez, F. et al.[33]
S. enterica SARA1	Beltran, P. et al.[71]
S. enterica Newport M11018046001A	Shariat, N. et al.[62]
S. enterica Enteriditis 05E01375	Shariat, N. et al.[62]
E. coli BL21-DE3 Cat# 70954-3	Millipore-Sigma

479
480
481

482 *Chemosensory injection rig assay (CIRA)*

483 CIRA was performed as described previously [1]. Briefly, an Eppendorf Femtotip 2 microcapillary
484 containing the treatment of interest was lowered into a pond of 50 µl of motile cells using a Sutter
485 micromanipulator. An injection flow of effector into the pond at approximately 300 fl per minute
486 was achieved using a Femtojet 4i set to P_c 35. Solubilized fecal treatments were prepared by
487 dissolving 1 g of commercially obtained human feces (Lee Biosolutions) in 10 ml of CB. The
488 solution was clarified by centrifugation at 10,000 g for 20 minutes, followed by sterile filtration
489 through a 0.2 µm filter. Treatment solutions of indole and L-Ser were also diluted into CB and
490 sterile-filtered before application. Videos were recorded using an inverted Nikon Ti2 microscope
491 with heated sample chamber at 37 ˚C.

492

493 *CIRA microgradient modeling*

494 Modeling the microgradient generated through CIRA was performed as described earlier [1], based
495 on the continual injection and diffusion of an effector from a fixed-point source. Briefly, diffusion
496 is modeled as a 3D process where the diffusing substance is gradually and continuously introduced
497 at a fixed point within a large surrounding fluid volume. The substance is prepared at a
498 concentration of M_s (typically between 0.5 µM and 5 mM) and injected at a volume rate of Q =
499 305.5 fl/min. The species then diffuses into the ambient fluid with a diffusion constant D:

500 $$C(r,t) = \frac{q}{4\pi Dr} erfc \frac{r}{2\sqrt{Dt}}$$

501 Here, r is the distance from the point source, t is the time from initial injections, q is the injection
502 rate of the species (equal to M_sQ), and C is the species concentration. In earlier work [1], we reported
503 using fluorescent dye that the concentrations predicted by this model appear to be accurate within
504 5% in the range of 70-270 µm from the source, whereas at distances less than 70 µm the measured
505 concentrations are about 10% lower than predicted. At the point where the effector treatment is
506 injected into the larger volume the local concentration drops precipitously, hence why the
507 concentration reported at distance 0 is not that of the concentration within the microcapillary.

508

509 *Isothermal titration calorimetry ligand binding studies (ITC)*

510 Purification of *S.* Typhimurium Tsr LBD was performed as described previously [1]. ITC
511 experiments were performed using a Microcal ITC200 instrument (GE Healthcare). Either 500 µM
512 indole or L-Ser was titrated in 2.5 µL injections into a 200 µL sample cell containing 50 µM Tsr

513 LBD. For the indole/L-Ser competition experiment, 500 μM indole was added to both the titrant
514 and sample cell, thus providing a constant excess background concentration of indole. For all
515 experimental conditions, blank titrations were also collected in which indole or L-Ser was titrated
516 into a cell containing buffer alone. All experiments were performed using thoroughly degassed
517 samples at 25 °C in 50 mM Tris, 150 mM NaCl, 1 mM EDTA, pH 7.5. The reference power was
518 set to 5 μcal/sec. The resulting power curves were integrated using the Origin analysis software
519 included with the instrument. The heat of dilution was subtracted from each point using the blank.
520 A single-site binding model was then fit to the data, floating parameters describing the binding
521 enthalpy (ΔH), equilibrium constant (K_D), and apparent binding stoichiometry (n). The instrument
522 software was used for this purpose.
523
524 *Quantification of indole and serine in human fecal samples*
525 Solubilized human feces was prepared as described above for CIRA and analyzed by mass
526 spectrometry to determine the molar serine content as a service through the University of
527 Washington Mass Spectrometry Center. This measurement reflects total serine, of which close to
528 100% is expected to be L-Ser [1]. As described in earlier work, the indole content of solubilized
529 human fecal samples was determined using a hydroxylamine-based calorimetric assay with
530 purified indole as a reference and standard [72].
531
532 *Explant infection assays*
533 Swine intestinal tissue was acquired from the descending colon of an 8-week-old animal, pursuant
534 to animal protocol ASAF #7128, approved through the Washington State University IACUC.
535 Before infection, the luminal side of an approximately 20 by 20 mm piece of swine intestinal
536 explant tissue was gently washed with PBS to remove fecal matter. Next, the tissue section was
537 bathed in 2 ml of chemoeffector solution (solubilized human fecal matter (Lee Biosolutions), a
538 mixture of 338 μM L-Ser and 862 μM indole, 338 μM L-Ser alone, 862 μM indole alone, or
539 chemotaxis buffer) in a 6-well tissue culture plate (Celltreat) and incubated at 4° C for 1 h. Then,
540 tissue was transferred to a 35 mm Mattek dish where the luminal side of the tissue was exposed to
541 a bacterial solution containing a 1:1 mixture (10^9 CFU each) of WT *S.* Typhimurium IR715 and
542 either the isogenic *tsr* or *cheY* mutant, suspended in CB at a volume of 300 μl. The tissue was then
543 incubated in the dish with the competing bacteria at 37 °C and 5% CO_2 for 1, 3, or 6 h. After, half

544 of the tissue was transferred into screwcap tubes containing 500 µl LB media and 5-10 2.3 mm
545 zirconia beads (BioSpec Products) on ice and homogenized using a Bead Mill 24 (Fisher
546 Scientific) at 6.5 m/s for 60 s, repeated four times. To enumerate the intracellular bacteria, the
547 other half of the tissue was washed in PBS and incubated in PBS containing 100 µg/ml gentamicin
548 for 1 h at 37 °C and 5% CO_2, then washed twice in PBS, as done previously [54,73,74]. The
549 homogenization process was then repeated for the gentamicin-treated tissue. CFUs were
550 enumerated by plating 10-fold dilutions on LB agar plates containing the appropriate antibiotic
551 [54,75]. Competitive index values were calculated by dividing the number of mutant CFUs by the
552 number of WT CFUs for each treatment and time point [76,77].
553
554 *Quantification of CIRA data*
555 Videos of chemotactic responses were quantified as described previously [1]. The number of cells
556 in each frame were calculated by determining a fluorescence intensity ratio per cell for frames pre-
557 treatment and extrapolated using the 'plot profile' function of ImageJ. The distribution of the
558 bacteria was calculated using the Radial Profile ImageJ plugin. Local background subtraction was
559 performed based on experiments with the non-chemotactic *cheY* strain to control for
560 autofluorescence in solubilized fecal samples.
561
562 *Statistical Analyses*
563 Competitive indices (CIs) for explant experiments were calculated for each treatment group at
564 each time point. Log-transformed CI values were obtained by taking the logarithm ($\log_{10}$) of the
565 original CI measurements. These log-transformed values were then subjected to statistical analysis.
566 First, a one-sample t-test was performed to determine whether the mean of the log-transformed
567 CIs significantly differed from zero. In cases where the assumption of normality was violated, the
568 non-parametric Wilcoxon rank sum test was applied as an alternative. Effect size was assessed
569 using Cohen's *d* and calculated using the same log-transformed CIs.
570
571 **Acknowledgments**
572 Funding for this research was provided by NIAID through awards 1K99AI148587 and
573 4R00AI148587-03, and funding from the College of Veterinary Medicine at Washington State
574 University to AB. Bacterial strains were provided by Nikki Shariat (University of Georgia,

575 Athens), Nkuchia Mikanatha and Pennsylvania NARMS and GenomeTrakr Programs, and
576 Andreas Bäumler (University of California, Davis). All research on human and animal samples
577 was performed in accordance with, and approval of, the Institutional Biosafety Committee and
578 Institutional Animal Care and Use Committee at Washington State University.
579
580 **Author Contributions**
581 K.F. performed the microgradient modeling and explant experiments. A.B. conducted the CIRA
582 experiments and purification of Tsr-LBD. Z.G. performed bacterial growth experiments. M.S. and
583 M.J.H. performed the ITC experiments. All authors contributed to data analyses and writing of the
584 manuscript.
585
586 **Declaration of Interests**
587 A.B. owns Amethyst Antimicrobials, LLC.
588
589 **Movie Figure legends**
590 **Movie 1.** Chemotactic response of *S.* Typhimurium IR715 to solubilized human feces, related to
591 Figure 2. Representative CIRA experiments showing *S.* Typhimurium IR715 WT and mutant
592 strains responding to a source over 300 s (shown at 10x speed) Viewable at:
593 https://www.youtube.com/watch?v=BqUcRN3YwjU
594
595 **Movie 2.** Chemotactic response of *S.* Typhimurium IR715 WT and chemotactic mutant strains to
596 solubilized human feces, related to Figure 3. Representative CIRA experiments showing
597 competition between *S.* Typhimurium IR715 (mPlum) and *cheY*, or *tsr*, as indicated (GFP), over
598 300 s. Viewable at: https://www.youtube.com/watch?v=D5JL46b4lsI
599
600 **Movie 3.** Chemotactic response of *S. enterica* clinical isolates to solubilized human feces, related
601 to Figure 3. Representative CIRA experiments showing competition between *S.* Typhimurium
602 IR715 (mPlum) and clinical isolates, as indicated (GFP), responding to a source of solubilized
603 human feces over 300 s. Viewable at: https://www.youtube.com/watch?v=dLsFDV0XgpY
604

605 **Movie 4.** Chemotactic response of *S.* Typhimurium IR715 to L-Ser and indole treatments, related
606 to Figure 4 and Figure S2. Representative CIRA experiments with treatment sources as indicated,
607 over 300 s. Viewable at: https://www.youtube.com/watch?v=bNQMqF2QMek
608
609

610 **References**

611 1. Glenn, S. J. *et al.* Bacterial vampirism mediated through taxis to serum. *eLife* **12**, RP93178
612 (2024).
613 2. Zhou, B., Szymanski, C. M. & Baylink, A. Bacterial chemotaxis in human diseases. *Trends*
614 *in Microbiology* **31**, 453–467 (2023).
615 3. Keegstra, J. M., Carrara, F. & Stocker, R. The ecological roles of bacterial chemotaxis.
616 *Nature Reviews Microbiology* (2022) doi:10.1038/s41579-022-00709-w.
617 4. Bi, S. & Sourjik, V. Stimulus sensing and signal processing in bacterial chemotaxis. *Current*
618 *Opinion in Microbiology* **45**, 22–29 (2018).
619 5. Matilla, M. A. & Krell, T. The effect of bacterial chemotaxis on host infection and
620 pathogenicity. *FEMS Microbiology Reviews* **42**, (2018).
621 6. Matilla, M. A., Gavira, J. A. & Krell, T. Accessing nutrients as the primary benefit arising
622 from chemotaxis. *Current Opinion in Microbiology* **75**, 102358 (2023).
623 7. Matilla, M. A. & Krell, T. Chemoreceptor-based signal sensing. *Current Opinion in*
624 *Biotechnology* **45**, 8–14 (2017).
625 8. Ortega, Á., Zhulin, I. B. & Krell, T. Sensory Repertoire of Bacterial Chemoreceptors.
626 *Microbiol Mol Biol Rev* **81**, e00033-17 (2017).
627 9. Rogers, A. W. L., Tsolis, R. M. & Bäumler, A. J. Salmonella versus the Microbiome.
628 *Microbiology and Molecular Biology Reviews* **85**, e00027-19 (2020).
629 10. Vos, W. M. de, Tilg, H., Hul, M. V. & Cani, P. D. Gut microbiome and health: mechanistic
630 insights. *Gut* **71**, 1020–1032 (2022).
631 11. Hill, J. H. *et al.* BefA, a microbiota-secreted membrane disrupter, disseminates to the
632 pancreas and increases β cell mass. *Cell Metabolism* **34**, 1779-1791.e9 (2022).

633 12. Yang, J. *et al.* Biphasic chemotaxis of *Escherichia coli* to the microbiota metabolite indole.
634 *Proc. Natl. Acad. Sci. U.S.A.* **117**, 6114–6120 (2020).
635 13. Livne, N. & Vaknin, A. Collective responses of bacteria to a local source of conflicting
636 effectors. *Sci Rep* **12**, 4928 (2022).
637 14. Keller, E. F. & Segel, L. A. Traveling bands of chemotactic bacteria: A theoretical analysis.
638 *Journal of Theoretical Biology* **30**, 235–248 (1971).
639 15. Adler, J. & Tso, W.-W. 'Decision'-Making in Bacteria: Chemotactic Response of
640 *Escherichia coli* to Conflicting Stimuli. *Science* **184**, 1292–1294 (1974).
641 16. Zhang, X. *et al.* Escape band in Escherichia coli chemotaxis in opposing attractant and
642 nutrient gradients. *Proc Natl Acad Sci U S A* **116**, 2253–2258 (2019).
643 17. Kalinin, Y., Neumann, S., Sourjik, V. & Wu, M. Responses of Escherichia coli Bacteria to
644 Two Opposing Chemoattractant Gradients Depend on the Chemoreceptor Ratio. *Journal of*
645 *Bacteriology* **192**, 1796 (2010).
646 18. Englert, D. L., Manson, M. D. & Jayaraman, A. Flow-Based Microfluidic Device for
647 Quantifying Bacterial Chemotaxis in Stable, Competing Gradients. *Appl Environ Microbiol*
648 **75**, 4557–4564 (2009).
649 19. Huang, J. Y., Sweeney, E. G., Guillemin, K. & Amieva, M. R. Multiple Acid Sensors
650 Control Helicobacter pylori Colonization of the Stomach. *PLOS Pathogens* **13**, e1006118
651 (2017).
652 20. Li, X., Zhang, B., Hu, Y. & Zhao, Y. New Insights Into Gut-Bacteria-Derived Indole and Its
653 Derivatives in Intestinal and Liver Diseases. *Front. Pharmacol.* **12**, 769501 (2021).
654 21. Lee, J.-H. & Lee, J. Indole as an intercellular signal in microbial communities. *FEMS*
655 *Microbiol Rev* **34**, 426–444 (2010).

656 22. Gupta, R. *et al.* Indole modulates cooperative protein–protein interactions in the flagellar
657 motor. *PNAS Nexus* **1**, pgac035 (2022).
658 23. Darkoh, C., Chappell, C., Gonzales, C. & Okhuysen, P. A Rapid and Specific Method for the
659 Detection of Indole in Complex Biological Samples. *Appl Environ Microbiol* **81**, 8093–8097
660 (2015).
661 24. Chappell, C. L. *et al.* Fecal Indole as a Biomarker of Susceptibility to Cryptosporidium
662 Infection. *Infect Immun* **84**, 2299–2306 (2016).
663 25. Ye, X. *et al.* Dual Role of Indoles Derived From Intestinal Microbiota on Human Health.
664 *Front. Immunol.* **13**, 903526 (2022).
665 26. Kumar, A. & Sperandio, V. Indole Signaling at the Host-Microbiota-Pathogen Interface.
666 *mBio* **10**, e01031-19 (2019).
667 27. Bansal, T. *et al.* Differential Effects of Epinephrine, Norepinephrine, and Indole on
668 *Escherichia coli* O157:H7 Chemotaxis, Colonization, and Gene Expression. *Infect Immun*
669 **75**, 4597–4607 (2007).
670 28. Kohli, N. *et al.* The microbiota metabolite indole inhibits Salmonella virulence: Involvement
671 of the PhoPQ two-component system. *PLOS ONE* **13**, e0190613 (2018).
672 29. Nikaido, E. *et al.* Effects of indole on drug resistance and virulence of Salmonella enterica
673 serovar Typhimurium revealed by genome-wide analyses. *Gut Pathog* **4**, 5 (2012).
674 30. Piñas, G. E., DeSantis, M. D., Cassidy, C. K. & Parkinson, J. S. Hexameric rings of the
675 scaffolding protein CheW enhance response sensitivity and cooperativity in Escherichia coli
676 chemoreceptor arrays. *Science Signaling* **15**, eabj1737 (2022).
677 31. Burt, A. *et al.* Complete structure of the chemosensory array core signalling unit in an E. coli
678 minicell strain. *Nat Commun* **11**, 743 (2020).

679 32. Chen, X., Bi, S., Ma, X., Sourjik, V. & Lai, L. Discovery of a New Chemoeffector for
680 Escherichia coli Chemoreceptor Tsr and Identification of a Molecular Mechanism of
681 Repellent Sensing. *ACS Bio Med Chem Au* **2**, 386–394 (2022).
682 33. Rivera-Chávez, F. *et al.* Salmonella Uses Energy Taxis to Benefit from Intestinal
683 Inflammation. *PLoS Pathog* **9**, e1003267 (2013).
684 34. Rivera-Chávez, F. *et al.* Energy Taxis toward Host-Derived Nitrate Supports a Salmonella
685 Pathogenicity Island 1-Independent Mechanism of Invasion. *mBio* **7**, e00960-16 (2016).
686 35. Gül, E. *et al.* Salmonella T3SS-2 virulence enhances gut-luminal colonization by enabling
687 chemotaxis-dependent exploitation of intestinal inflammation. *Cell Rep* **43**, 113925 (2024).
688 36. Winter, S. E., Lopez, C. A. & Bäumler, A. J. The dynamics of gut-associated microbial
689 communities during inflammation. *EMBO Reports* **14**, 319–327 (2013).
690 37. Winter, S. E. *et al.* Gut inflammation provides a respiratory electron acceptor for Salmonella.
691 *Nature* **467**, 426–429 (2010).
692 38. Cooper, K. G. *et al.* Regulatory protein HilD stimulates Salmonella Typhimurium
693 invasiveness by promoting smooth swimming via the methyl-accepting chemotaxis protein
694 McpC. *Nat Commun* **12**, 348 (2021).
695 39. Vega, N. M., Allison, K. R., Samuels, A. N., Klempner, M. S. & Collins, J. J. *Salmonella*
696 *typhimurium* intercepts *Escherichia coli* signaling to enhance antibiotic tolerance. *Proc. Natl.*
697 *Acad. Sci. U.S.A.* **110**, 14420–14425 (2013).
698 40. Roager, H. M. & Licht, T. R. Microbial tryptophan catabolites in health and disease. *Nat*
699 *Commun* **9**, 3294 (2018).
700 41. Chowdhury, R., Pavinski Bitar, P. D., Chapman, H. M. & Altier, C. Salmonella Invasion Is
701 Controlled by Competition among Intestinal Chemical Signals. *mBio* **14**, e00012-23 (2023).

702 42. Ehrhardt, K. & Grassl, G. A. Mouse Model to Study Salmonella-Induced Colitis. *Methods*
703 *Mol Biol* **2427**, 201–213 (2022).
704 43. Grassl, G. A., Valdez, Y., Bergstrom, K. S. B., Vallance, B. A. & Finlay, B. B. Chronic
705 enteric salmonella infection in mice leads to severe and persistent intestinal fibrosis.
706 *Gastroenterology* **134**, 768–780 (2008).
707 44. Radlinski, L. C. *et al.* Salmonella virulence factors induce amino acid malabsorption in the
708 ileum to promote ecosystem invasion of the large intestine. *Proceedings of the National*
709 *Academy of Sciences* **121**, e2417232121 (2024).
710 45. Kronsteiner, B. *et al.* Helicobacter pylori Infection in a Pig Model Is Dominated by Th1 and
711 Cytotoxic CD8 $^{+}$ T Cell Responses. *Infect Immun* **81**, 3803–3813 (2013).
712 46. Smith, A. C. & Swindle, M. M. Preparation of Swine for the Laboratory. *ILAR Journal* **47**,
713 358–363 (2006).
714 47. Poutahidis, T. *et al. Helicobacter pylori* -induced Gastritis in Experimentally Infected
715 Conventional Piglets. *Vet Pathol* **38**, 667–678 (2001).
716 48. Boyen, F. *et al.* Porcine *in vitro* and *in vivo* models to assess the virulence of *Salmonella*
717 *enterica* serovar Typhimurium for pigs. *Lab Anim* **43**, 46–52 (2009).
718 49. Boyen, F. *et al.* Coated fatty acids alter virulence properties of Salmonella Typhimurium and
719 decrease intestinal colonization of pigs. *Veterinary Microbiology* **132**, 319–327 (2008).
720 50. Köppen, K. *et al.* Ex vivo infection model for Francisella using human lung tissue. *Front.*
721 *Cell. Infect. Microbiol.* **13**, (2023).
722 51. Bomjan, R., Zhang, M. & Zhou, D. YshB Promotes Intracellular Replication and Is Required
723 for Salmonella Virulence. *Journal of Bacteriology* **201**, 10.1128/jb.00314-19 (2019).

724 52. Birhanu, B. T., Park, N.-H., Lee, S.-J., Hossain, M. A. & Park, S.-C. Inhibition of
725 Salmonella Typhimurium adhesion, invasion, and intracellular survival via treatment with
726 methyl gallate alone and in combination with marbofloxacin. *Veterinary Research* **49**, 101
727 (2018).
728 53. MacBeth, K. J. & Lee, C. A. Prolonged inhibition of bacterial protein synthesis abolishes
729 Salmonella invasion. *Infect Immun* **61**, 1544–1546 (1993).
730 54. Sharma, A. & Puhar, A. Gentamicin Protection Assay to Determine the Number of
731 Intracellular Bacteria during Infection of Human TC7 Intestinal Epithelial Cells by Shigella
732 flexneri. *BIO-PROTOCOL* **9**, (2019).
733 55. Kitamoto, S. *et al.* Dietary l-serine confers a competitive fitness advantage to
734 Enterobacteriaceae in the inflamed gut. *Nature Microbiology* **5**, 116–125 (2020).
735 56. Sugihara, K. & Kamada, N. THE ROLE OF DIETARY L-SERINE IN THE REGULATION
736 OF INTESTINAL MUCUS BARRIER DURING INFLAMMATION. *Inflammatory Bowel*
737 *Diseases* **26**, S42–S42 (2020).
738 57. Ranque, C. L. *et al.* Examination of Carbohydrate Products in Feces Reveals Potential
739 Biomarkers Distinguishing Exclusive and Nonexclusive Breastfeeding Practices in Infants. *J*
740 *Nutr* **150**, 1051–1057 (2020).
741 58. Ke, Z., Lu, Z., Li, Q. & Tong, W. Intestinal glucose excretion: A potential mechanism for
742 glycemic control. *Metabolism* **152**, 155743 (2024).
743 59. Larke, J. A. *et al.* Dietary Intake of Monosaccharides from Foods is Associated with
744 Characteristics of the Gut Microbiota and Gastrointestinal Inflammation in Healthy US
745 Adults. *The Journal of Nutrition* **153**, 106–119 (2023).

746 60. Shen, X. *et al.* Asparagine, colorectal cancer, and the role of sex, genes, microbes, and diet:
747 A narrative review. *Front Mol Biosci* **9**, 958666 (2022).
748 61. Yoo, W. *et al. Salmonella* Typhimurium expansion in the inflamed murine gut is dependent
749 on aspartate derived from ROS-mediated microbiota lysis. *Cell Host & Microbe* **32**, 887-
750 899.e6 (2024).
751 62. Shariat, N. *et al.* Subtyping of Salmonella enterica Serovar Newport Outbreak Isolates by
752 CRISPR-MVLST and Determination of the Relationship between CRISPR-MVLST and
753 PFGE Results. *J Clin Microbiol* **51**, 2328–2336 (2013).
754 63. Ferrari, R. G. *et al.* Worldwide Epidemiology of *Salmonella* Serovars in Animal-Based
755 Foods: a Meta-analysis. *Appl Environ Microbiol* **85**, e00591-19 (2019).
756 64. Gavira, J. A. *et al.* How Bacterial Chemoreceptors Evolve Novel Ligand Specificities. *mBio*
757 **11**, e03066-19 (2020).
758 65. Matilla, M. A., Ortega, Á. & Krell, T. The role of solute binding proteins in signal
759 transduction. *Computational and Structural Biotechnology Journal* **19**, 1786–1805 (2021).
760 66. Chimerel, C., Field, C. M., Piñero-Fernandez, S., Keyser, U. F. & Summers, D. K. Indole
761 prevents Escherichia coli cell division by modulating membrane potential. *Biochim Biophys*
762 *Acta* **1818**, 1590–1594 (2012).
763 67. Melander, R. J., Minvielle, M. J. & Melander, C. Controlling bacterial behavior with indole-
764 containing natural products and derivatives. *Tetrahedron* **70**, 6363–6372 (2014).
765 68. Moore, J. P., Kamino, K., Kottou, R., Shimizu, T. S. & Emonet, T. Signal integration and
766 adaptive sensory diversity tuning in *Escherichia coli* chemotaxis. *Cell Systems* **15**, 628-
767 638.e8 (2024).

768 69. Huang, J. Y. *et al.* Chemodetection and Destruction of Host Urea Allows Helicobacter pylori
769 to Locate the Epithelium. *Cell Host & Microbe* **18**, 147–156 (2015).
770 70. Khan, S. & Trentham, D. R. Biphasic Excitation by Leucine in Escherichia coli Chemotaxis.
771 *J Bacteriol* **186**, 588–592 (2004).
772 71. Beltran, P. *et al.* Reference collection of strains of the Salmonella typhimurium complex
773 from natural populations. *Journal of General Microbiology* **137**, 601–606 (1991).
774 72. Sugihara, K. *et al.* Mucolytic bacteria license pathobionts to acquire host-derived nutrients
775 during dietary nutrient restriction. *Cell Reports* **40**, 111093 (2022).
776 73. Chandra, K. Gentamicin Protection assay (Intracellular Survival Assay) for Salmonella
777 Typhimurium/Typhi v1. Preprint at https://doi.org/10.17504/protocols.io.b4zmqx46 (2022).
778 74. Rivera Calo, J., Rubinelli, P. M. & Ricke, S. C. Gentamicin Susceptibility and Comparison
779 of Adhesion and Invasion of Caco-2 and HD11 Cell Lines by Salmonella enterica Serotypes.
780 *Applied Sciences* **14**, 3305 (2024).
781 75. Ben-David, A. & Davidson, C. E. Estimation method for serial dilution experiments. *Journal*
782 *of Microbiological Methods* **107**, 214–221 (2014).
783 76. Macho, A. P., Zumaquero, A., Ortiz-Martín, I. & Beuzón, C. R. Competitive index in mixed
784 infections: a sensitive and accurate assay for the genetic analysis of *Pseudomonas syringae* –
785 plant interactions. *Molecular Plant Pathology* **8**, 437–450 (2007).
786 77. Auerbuch, V., Lenz, L. L. & Portnoy, D. A. Development of a competitive index assay to
787 evaluate the virulence of Listeria monocytogenes actA mutants during primary and
788 secondary infection of mice. *Infect Immun* **69**, 5953–5957 (2001).
789
790
791

792 **Supplemental Information**

793 **Table S1.** Summary of prior studies related to indole chemotaxis, related to Figure 1.

Species, Strain(s)	Indole Treatment [a]	Reported Response [b]	Experimental Method(s)	Chemotaxis & Motility Proteins Involved in Response	Ref.
E. coli, strain RP437	≤1 mM >1 mM	chemorepulsion chemoattraction	tethered cell assay [c]	Tsr, Tar	12
E. coli, strain MG1655	1 mM ± 0.5-0.1 mM L-Ser	"bet-hedging" [d]	diffusion-based assay into long channel with fluorescent imaging	Tar, Tsr	13
E. coli, strain RP437	500 µM	chemorepulsion, overridden in presence of 500 µM Autoinducer-2	flow-based microfluidic chemotaxis device coupled to a gradient generator	Tar, Tsr	18
E. coli, strain RP437	≤1 mM >1 mM	decreased motility slower flagellar rotation	tethered cell assay [c]	Non-CheY dependent	22
E. coli, strain O157:H7 CDC EDL933	500 µM	chemorepulsion	agarose plug chemotaxis assay imaged every 5 minutes for 30 minutes	MotB and FliD	27
S. Typhimurium, strain ATCC14028s	1 mM	decreased motility	swimming motility agar plates [c]	MotA	28
S. Typhimurium, strain ATCC14028s	1 mM	decreased motility	swimming motility agar plates [c]	FlhC	29

794

795

796 [a] Source concentration, or ranges, used in experiment.

797 [b] The motility or chemotactic response as reported by the study authors; note that some methods
798 employed may not be able to distinguish between responses as a consequence bacterial growth
799 versus chemotaxis.

800 [c] The assay may have limitations in its ability to report on either rapid temporal responses, or
801 localization to or from an effector source.

802 [d] In this work, we refer to behaviors of this type as "chemohalation" to be similar to the widely-
803 used terms chemoattraction and chemorepulsion.

804

805 **Data S1.** Enumeration of colony-forming units (CFUs) from explant studies.

806

807

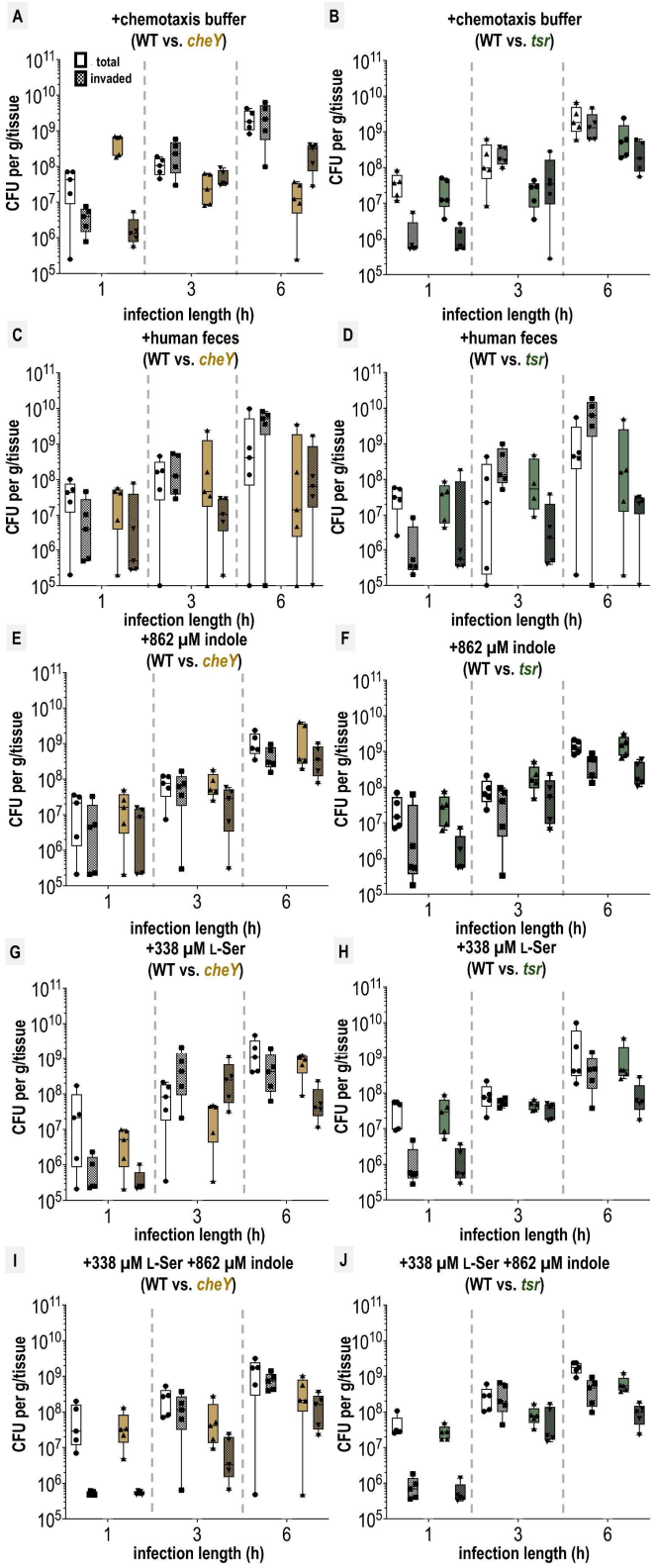

Fig. S1. Colony-forming units (CFU) recovered from swine colonic explant infections, related to Figure 1. Shown are disaggregated CFU enumerations for each co-infection experiment with *S.* Typhimurium IR715 WT and mutant strains following tissue treatments, as indicated. CFUs extracted either using the entire tissue homogenate (total) or extracted from tissue treated with a gentamicin wash to kill exterior non-invaded cells (invaded) are noted separately (see Materials & Methods). Each data point represents CFUs recovered from a single explant experiment (n=5). Box and whisker plots represent the sample median (line), the edges are the upper and lower quartiles, and whiskers extend to the max and min values. The limit of detection was 1 x 10^5 CFUs. Samples with no CFUs detected are noted on the plot at this limit.

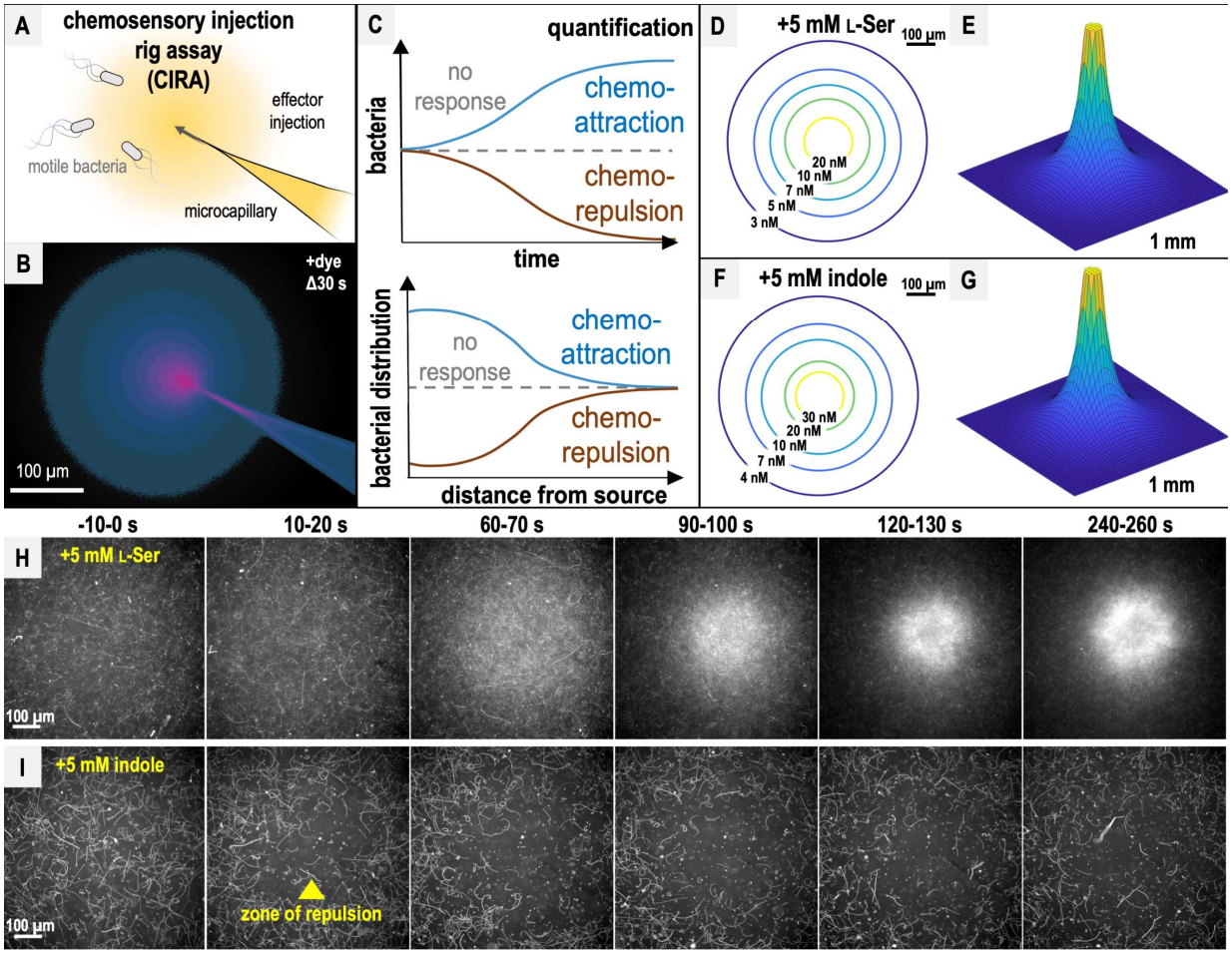

Fig. S2. Chemotactic responses to L-Ser or indole, related to Figure 2. A. CIRA experimental design. B. CIRA microgradient diffusion model, simulated with a source of 1.13 mM A488 dye after 30 s of injection. Image rendered on a pink (100% source concentration)-blue-black (0%) color intensity scale, based on previous work [1]. C. CIRA quantification overview, with blue lines corresponding to chemoattraction, null chemotactic response corresponding to gray dashed lines, and chemorepulsion corresponding to brown lines. D-G. Microgradient models of the local effector concentration for treatments with 5 mM L-Ser or indole, respectively, at Δ300 s. Color gradient corresponds to gradually decreasing effector concentrations from yellow to blue. H-I. Representative 10 s max projections of *S.* Typhimurium IR715 response to sources of L-Ser (strong chemoattraction) or indole (strong chemorepulsion) using CIRA. The glass microcapillary that injects the treatment solution is centered within the field of view. Note that cells contain a plasmid expressing mPlum (see Materials & Methods), and fluorescence data are collected in the far-red channel, so the glass microcapillary is poorly visible.

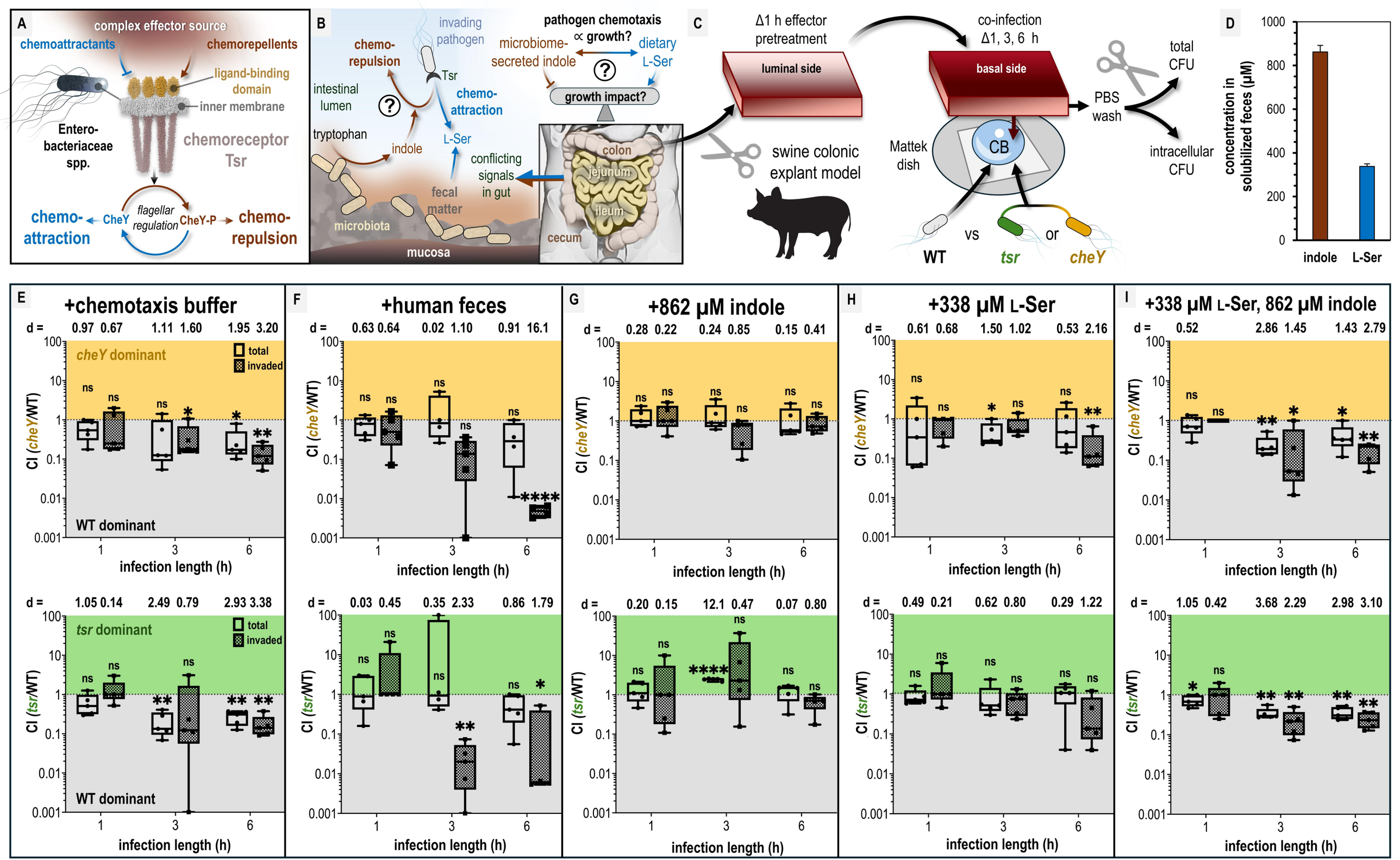
A
complex effector source
chemoattractants
chemorepellents
ligand-binding domain
inner membrane
Entero-bacteriaceae spp.
chemoreceptor Tsr
chemo-attraction
CheY
flagellar regulation
CheY-P
chemo-repulsion
B
invading pathogen
chemo-repulsion
Tsr
intestinal lumen
chemo-attraction
tryptophan
indole
L-Ser
conflicting signals in gut
fecal matter
microbiota
mucosa
pathogen chemotaxis ∝ growth?
microbiome-secreted indole
dietary L-Ser
growth impact?
colon
jejunum
ileum
cecum
C
Δ1 h effector pretreatment
luminal side
swine colonic explant model
co-infection Δ1, 3, 6 h
basal side
Mattek dish
CB
PBS wash
total CFU
intracellular CFU
WT
vs
tsr
or
cheY
D
concentration in solubilized feces (µM)
indole
L-Ser
E
+chemotaxis buffer
d = 0.97 0.67 1.11 1.60 1.95 3.20
cheY dominant
total
invaded
WT dominant
CI (cheY/WT)
infection length (h)
d = 1.05 0.14 2.49 0.79 2.93 3.38
tsr dominant
WT dominant
CI (tsr/WT)
F
+human feces
d = 0.63 0.64 0.02 1.10 0.91 16.1
d = 0.03 0.45 0.35 2.33 0.86 1.79
G
+862 µM indole
d = 0.28 0.22 0.24 0.85 0.15 0.41
d = 0.20 0.15 12.1 0.47 0.07 0.80
H
+338 µM L-Ser
d = 0.61 0.68 1.50 1.02 0.53 2.16
d = 0.49 0.21 0.62 0.80 0.29 1.22
I
+338 µM L-Ser, 862 µM indole
d = 0.52 2.86 1.45 1.43 2.79
d = 1.05 0.42 3.68 2.29 2.98 3.10

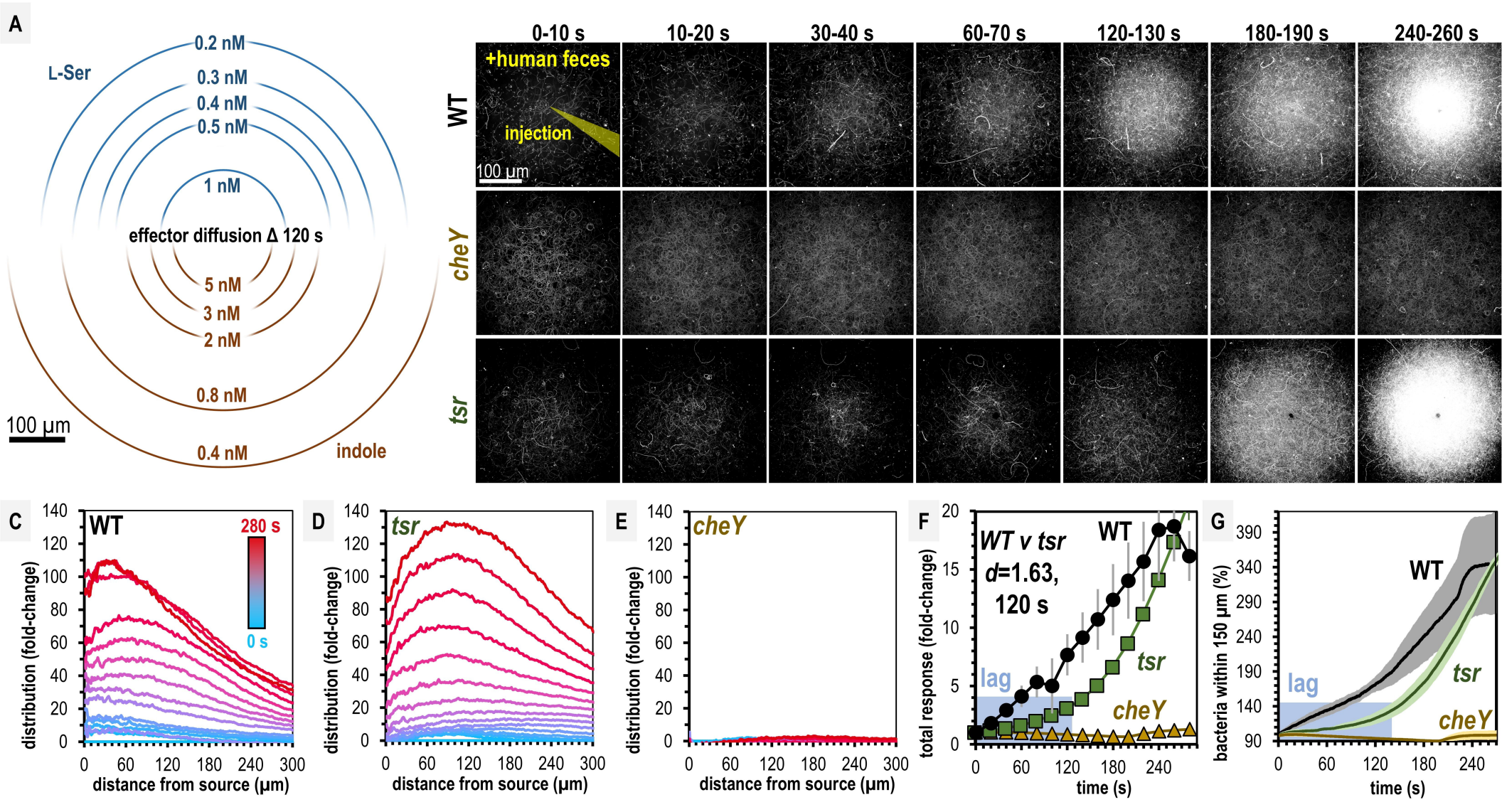
A
L-Ser
0.2 nM
0.3 nM
0.4 nM
0.5 nM
1 nM
effector diffusion Δ 120 s
5 nM
3 nM
2 nM
0.8 nM
0.4 nM
indole
100 µm
0-10 s
10-20 s
30-40 s
60-70 s
120-130 s
180-190 s
240-260 s
WT
cheY
tsr
+human feces
injection
100 µm
C
WT
280 s
0 s
distribution (fold-change)
distance from source (µm)
D
tsr
E
cheY
F
WT v tsr
d=1.63,
120 s
WT
tsr
cheY
lag
total response (fold-change)
time (s)
G
WT
tsr
cheY
lag
bacteria within 150 µm (%)
time (s)

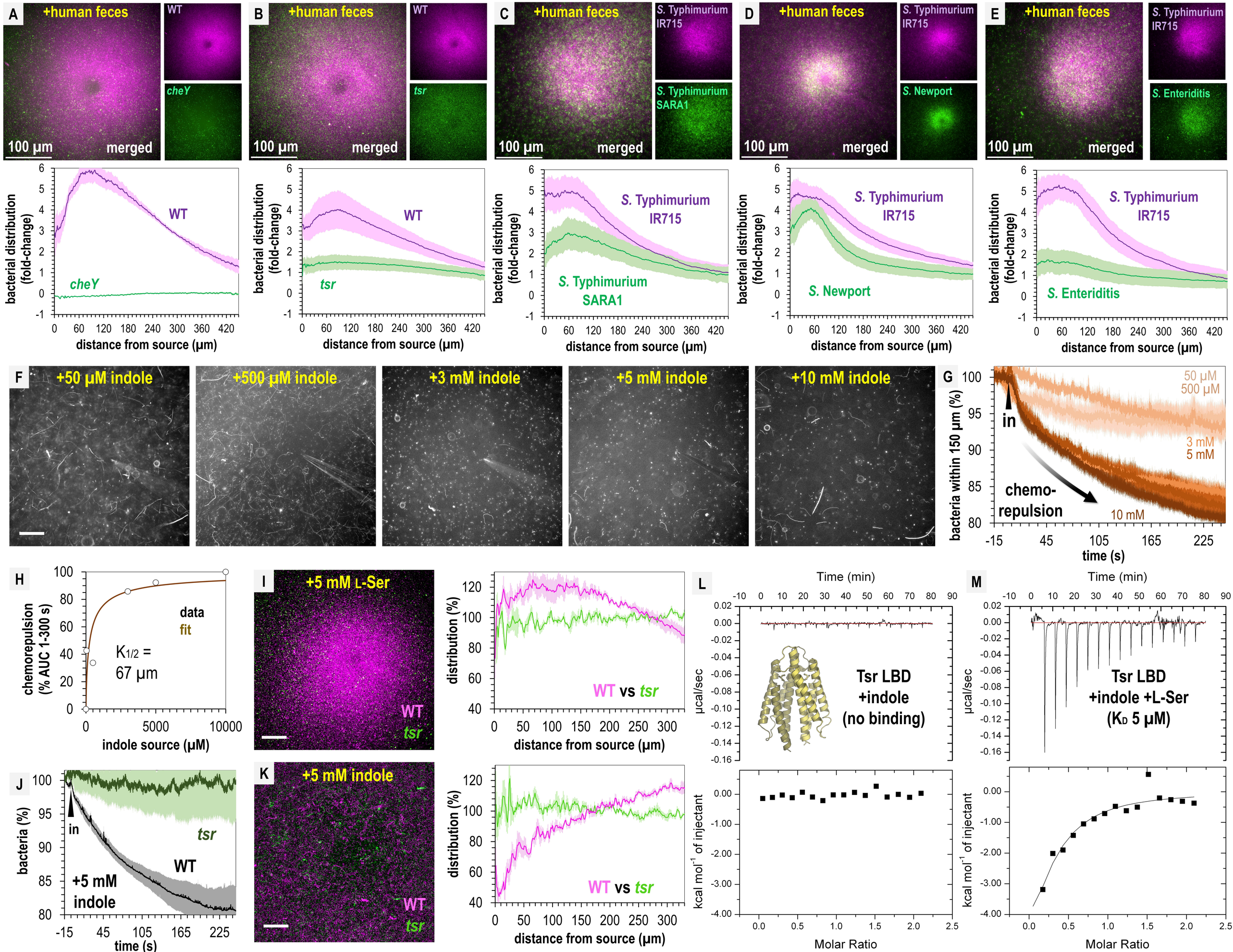
A
+human feces
WT
cheY
100 µm
merged
bacterial distribution (fold-change)
distance from source (µm)
B
+human feces
WT
tsr
C
+human feces
S. Typhimurium IR715
S. Typhimurium SARA1
D
+human feces
S. Typhimurium IR715
S. Newport
E
+human feces
S. Typhimurium IR715
S. Enteriditis
F
+50 µM indole
+500 µM indole
+3 mM indole
+5 mM indole
+10 mM indole
G
bacteria within 150 µm (%)
time (s)
in
chemo-repulsion
50 µM
500 µM
3 mM
5 mM
10 mM
H
chemorepulsion (% AUC 1-300 s)
indole source (µM)
data
fit
K1/2 = 67 µm
I
+5 mM L-Ser
WT
tsr
distribution (%)
WT vs tsr
J
bacteria (%)
time (s)
in
tsr
WT
+5 mM indole
K
+5 mM indole
L
Time (min)
µcal/sec
Tsr LBD +indole (no binding)
kcal mol-1 of injectant
Molar Ratio
M
Tsr LBD +indole +L-Ser (KD 5 µM)

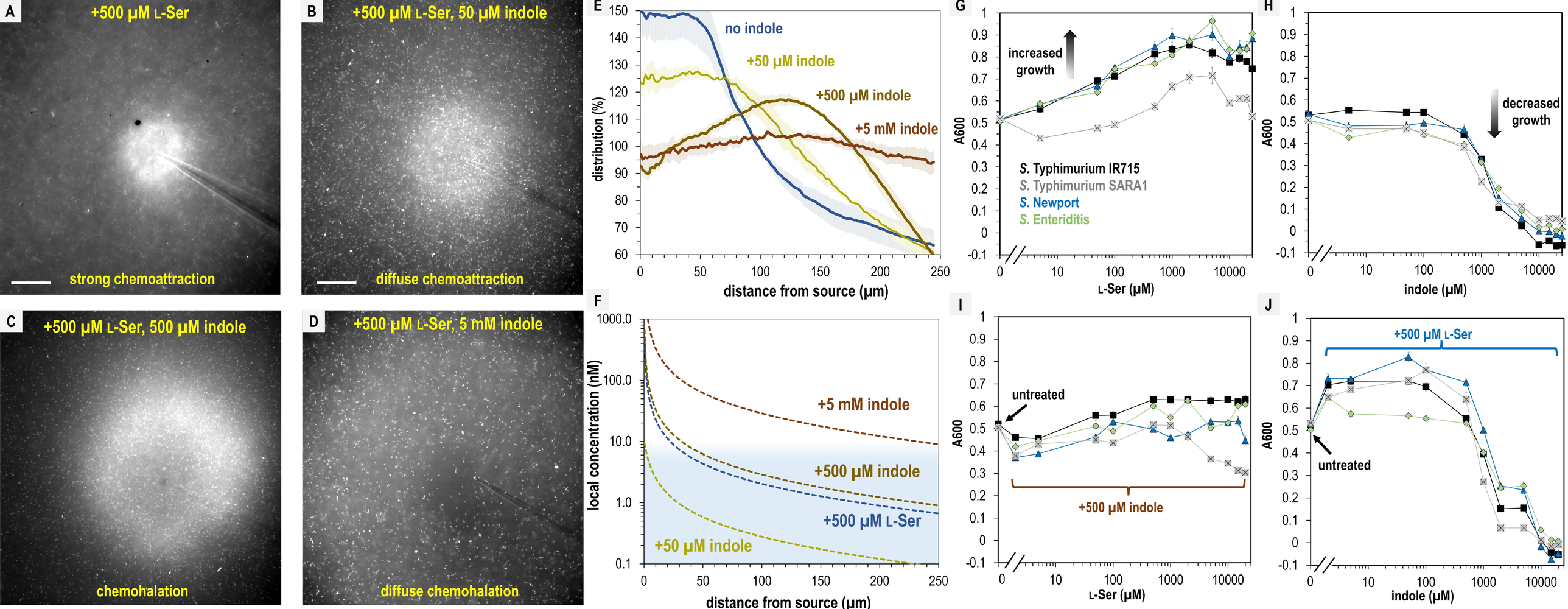
A
+500 μM L-Ser
strong chemoattraction
B
+500 μM L-Ser, 50 μM indole
diffuse chemoattraction
C
+500 μM L-Ser, 500 μM indole
chemohalation
D
+500 μM L-Ser, 5 mM indole
diffuse chemohalation
E
no indole
+50 μM indole
+500 μM indole
+5 mM indole
distribution (%)
distance from source (μm)
F
+5 mM indole
+500 μM indole
+500 μM L-Ser
+50 μM indole
local concentration (nM)
distance from source (μm)
G
increased growth
S. Typhimurium IR715
S. Typhimurium SARA1
S. Newport
S. Enteriditis
A600
L-Ser (μM)
H
decreased growth
A600
indole (μM)
I
untreated
+500 μM indole
A600
L-Ser (μM)
J
+500 μM L-Ser
untreated
A600
indole (μM)

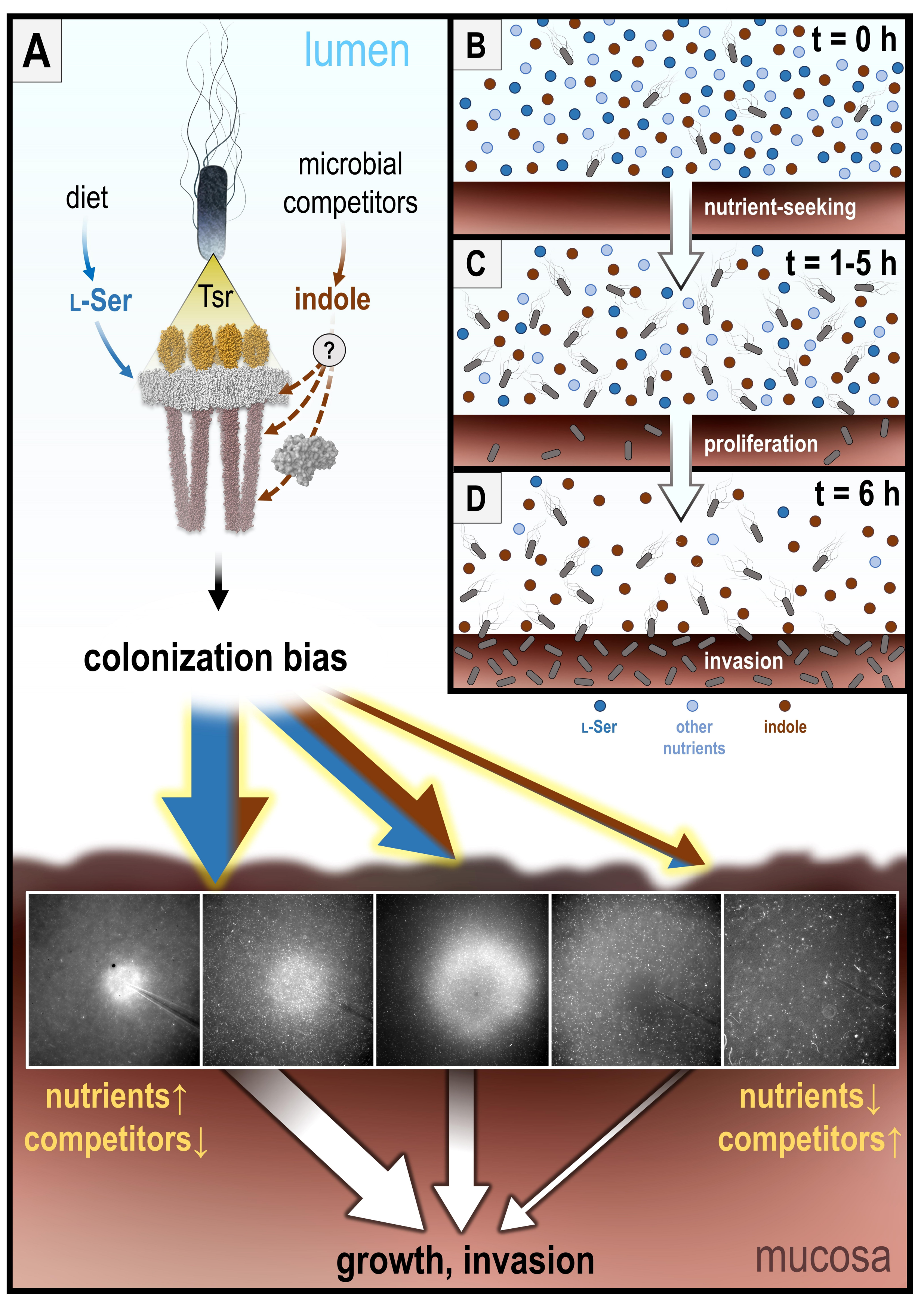
A
lumen
diet
L-Ser
Tsr
microbial
competitors
indole
?
colonization bias
B
t = 0 h
nutrient-seeking
C
t = 1-5 h
proliferation
D
t = 6 h
invasion
L-Ser
other
nutrients
indole
nutrients↑
competitors↓
nutrients↓
competitors↑
growth, invasion
mucosa